


RESEARCH ARTICLE

Open Access

METTL3-dependent RNA m⁶A dysregulation contributes to neurodegeneration in Alzheimer's disease through aberrant cell cycle events



Fanpeng Zhao¹, Ying Xu², Shichao Gao², Lixia Qin^{1,3}, Quillan Austria¹, Sandra L. Siedlak¹, Kinga Pajdzik⁴, Qing Dai⁴, Chuan He^{4,5}, Wenzhang Wang¹, James M. O'Donnell², Beisha Tang³ and Xiongwei Zhu^{1*} 

Abstract

Background: N⁶-methyladenosine (m⁶A) modification of RNA influences fundamental aspects of RNA metabolism and m⁶A dysregulation is implicated in various human diseases. In this study, we explored the potential role of RNA m⁶A modification in the pathogenesis of Alzheimer disease (AD).

Methods: We investigated the m⁶A modification and the expression of m⁶A regulators in the brain tissues of AD patients and determined the impact and underlying mechanism of manipulated expression of m⁶A levels on AD-related deficits both in vitro and in vivo.

Results: We found decreased neuronal m⁶A levels along with significantly reduced expression of m⁶A methyltransferase like 3 (METTL3) in AD brains. Interestingly, reduced neuronal m⁶A modification in the hippocampus caused by METTL3 knockdown led to significant memory deficits, accompanied by extensive synaptic loss and neuronal death along with multiple AD-related cellular alterations including oxidative stress and aberrant cell cycle events in vivo. Inhibition of oxidative stress or cell cycle alleviated shMettl3-induced apoptotic activation and neuronal damage in primary neurons. Restored m⁶A modification by inhibiting its demethylation in vitro rescued abnormal cell cycle events, neuronal deficits and death induced by METTL3 knockdown. Soluble A β oligomers caused reduced METTL3 expression and METTL3 knockdown exacerbated while METTL3 overexpression rescued A β -induced synaptic PSD95 loss in vitro. Importantly, METTL3 overexpression rescued A β -induced synaptic damage and cognitive impairment in vivo.

Conclusions: Collectively, these data suggested that METTL3 reduction-mediated m⁶A dysregulation likely contributes to neurodegeneration in AD which may be a therapeutic target for AD.

Keywords: RNA m⁶A modification, RNA methylation, METTL3, Alzheimer's disease, Aberrant cell cycle events, Apoptosis

Background

Alzheimer's disease (AD) is a degenerative brain disorder and the most prevalent form of dementia with progressive synaptic dysfunction, neuronal loss and memory

impairments [1]. Clinically expressed AD begins with the mild cognitive impairment (MCI) phase, which represents the earliest symptomatic stage to AD and other dementias [1–3]. Currently available FDA-approved treatments can only provide limited symptomatic alleviation. While more recent clinical trials are aimed at preventing disease progression in at-risk individuals or early stage in disease, none has been successful and many have been halted which is largely due to

* Correspondence: xiongwei.zhu@case.edu

¹Department of Pathology, Case Western Reserve University, 2103 Cornell Road, Cleveland, OH 44106, USA

Full list of author information is available at the end of the article



© The Author(s). 2021 **Open Access** This article is licensed under a Creative Commons Attribution 4.0 International License, which permits use, sharing, adaptation, distribution and reproduction in any medium or format, as long as you give appropriate credit to the original author(s) and the source, provide a link to the Creative Commons licence, and indicate if changes were made. The images or other third party material in this article are included in the article's Creative Commons licence, unless indicated otherwise in a credit line to the material. If material is not included in the article's Creative Commons licence and your intended use is not permitted by statutory regulation or exceeds the permitted use, you will need to obtain permission directly from the copyright holder. To view a copy of this licence, visit <http://creativecommons.org/licenses/by/4.0/>. The Creative Commons Public Domain Dedication waiver (<http://creativecommons.org/publicdomain/zero/1.0/>) applies to the data made available in this article, unless otherwise stated in a credit line to the data.

incomplete understanding of pathogenic mechanisms underlying synaptic dysfunction, neuronal loss and memory deficits in AD. Early onset AD which occurs in people before age of 65 is caused by mutations in APP, PS1 or PS2, but the cause of far more common late onset AD with age of onset older than 65 remains elusive. It is believed that a combination of genetics, environmental and lifestyle factors affect ones' risk of developing AD [4]. Therefore, in addition to genetic studies, there are expanding number of studies on a potential role of epigenetic modifications in AD [5, 6]. These studies largely focused on epigenetic DNA modifications and provided important insights into the complex etiology of the late-onset AD.

Most recently, it has become clear that RNA modifications could also lead to alterations in gene expression [7] which allows extra layers of regulation of gene-environmental interaction. N⁶-methyladenosine (m⁶A) is the most common internal modification in multiple RNA species [8]. Reversible RNA m⁶A modification is dynamically modulated by the methyltransferases "writers" and demethylases "erasers" [9, 10]. RNA m⁶A is deposited by a multicomponent methyltransferase complex consisting of methyltransferase like 3 (METTL3) [11], METTL14 [12, 13], and Wilms Tumor 1 Associated Protein (WTAP) [14, 15]. Fat mass and obesity associated protein (FTO) [16] and α -ketoglutarate-dependent dioxygenase alkB homolog 5 (ALKBH5) [17] are responsible for m⁶A removal to achieve dynamic regulation. m⁶A modification exerts its effects by recruiting m⁶A-binding proteins to regulate RNA metabolism. It can be recognized by "readers" containing the YTH (YT521-B homology) domain [18], such as YTHDF1 [19], YTHDF2 [20] and YTHDF3 [21, 22]. A growing body of evidence indicates that RNA m⁶A methylation is involved in diverse biological processes including stress response regulation [23], adult neurogenesis [24], axon regeneration [25], synaptic function [26], and cognitive function [27–30]. Specifically, interrupting m⁶A-mediated regulation by knockdown of m⁶A readers in hippocampus altered synaptic gene expression and induced memory dysfunction [26, 29]. Meanwhile, reduction of m⁶A eraser FTO in hippocampus modulates learning process and memory formation in mice [27, 28]. The efficacy of hippocampus-dependent memory consolidation is regulated by METTL3 through promoting the translation of neuronal early-response genes [30]. However, the potential role of RNA m⁶A modification in AD and neurodegenerative diseases is largely unexplored.

In the present study, we showed that m⁶A-related regulators and neuronal RNA m⁶A modification were decreased in AD brains. Decreased m⁶A modification by METTL3 knockdown in the hippocampus in vivo resulted in elevated oxidative stress, aberrant cell cycle events, activation of apoptosis and neurodegeneration as well as cognitive deficits similar to that of AD. We found cell cycle inhibition or antioxidant could rescue

METTL3 knockdown-induced neuronal deficits and neurodegeneration in vitro. Restored m⁶A modification by inhibiting its demethylation in vitro also rescued neuronal deficits and death induced by METTL3 knockdown. Thus, our results together suggest a potential role for RNA m⁶A dysregulation in the AD pathogenesis as well as its possible involvement in other neurodegenerative diseases.

Materials and methods

Postmortem brain samples

Cortical and hippocampal brain samples from postmortem AD and age-matched controls were collected at time of autopsy and stored at -80°C in the lab as described previously [31]. Brain samples were obtained under approved IRB protocols from the Brain Bank at Case Western Reserve University (CWRU). All AD cases were categorized based on clinical criteria established by CERAD and an NIA consensus panel [32, 33] and histopathologically confirmed according to the NINCDS-ADRDA criteria. Case information was provided in Table 1. Representative pictures of immunohistochemistry (IHC) for phosphorylated tau (using AT8 antibody) of an AD and control case were provided in Fig. S1A-C. No differences in post-mortem interval and ages between the AD and control tissues were observed in this study. The middle temporal gyrus samples from MCI and matched control cases were provided by Dr. Shi Jiong and Tom Beach (Barrow Neurological Institute). Human tissues were homogenized with RIPA lysis buffer for immunoblot analysis or fixed for immunohistochemical analysis.

Cell culture, plasmids, and treatment

Mouse N2a cells (CCL-131) were purchased from ATCC. The cells were grown in Opti-MEM I medium (Invitrogen, Carlsbad, CA, 31985088), supplemented with 5% (v/v) fetal bovine serum (Gibco, Carlsbad, CA, 10438026) and 1% penicillin-streptomycin (Gibco, Carlsbad, CA, 15140122). Primary neurons from E16 ~ 18 rat cortex (Charles River Laboratories) were seeded at 25000–40000 cells per well on coverslips or in 24-well plates coated with poly-D-lysine (Sigma, St. Louis, MO, P6407) in neurobasal medium (Gibco, Carlsbad, CA, 21103049) supplemented with 2% B27 / GlutaMAX (Gibco, Carlsbad, CA, 17504044 / 35050061). Half culture medium was changed every 3–4 days for primary neuronal cultures. All cultures were kept at 37°C in a humidified 5% CO_2 -containing atmosphere. Soluble amyloid- β oligomers (A β Os) were prepared using A β_{1-42} peptide (California Peptide) as described before [31].

Mice and surgery

Equal number of male and female wild-type C57BL/6 mice (000664) from Jackson Laboratory were used at 9–

Table 1 Clinical characteristics of AD and control cases

| Case ID | Age | Gender | Diagnosis | Braak stage |
|---------|-----|--------|-----------|-------------|
| AD 1 | 65 | male | AD | Braak VI |
| AD 2 | 68 | male | AD | Braak VI |
| AD 3 | 76 | male | AD | Braak V |
| AD 4 | 85 | male | AD | Braak VI |
| AD 5 | 86 | female | AD | Braak V/VI |
| AD 6 | 90 | female | AD | Braak VI |
| Ctrl 1 | 63 | male | control | none |
| Ctrl 2 | 84 | male | control | none |
| Ctrl 3 | 70 | male | control | none |
| Ctrl 4 | 76 | male | control | none |
| Ctrl 5 | 83 | female | control | none |
| Ctrl 6 | 85 | female | control | none |

10 weeks of age for AAV infusion experiments and A β O treatment experiment. All procedures were approved by the Institutional Animal Care and Use Committee of CWRU (protocol# 2017–0028) and SUNY-Buffalo (protocol# PHC14093Y). All the mice were maintained under constant environmental conditions in the Animal Research Center with free access to food and water. Mice were randomly assigned to the various experimental groups and randomly selected for the stereotaxic infusion and behavioral experiments.

The shRNAs in this study were generated based on pAAV-U6-GFP expression vector (Cell Biolabs). The targeting sequence (GCTCTATCCAGGCCCATAA) of shRNA was designed for both mouse and rat *Mettl3* mRNA and knockdown effect was verified in indicated cell lines. Nonfunctional shRNA (TAAGGTTAAGTCGCCCTCG) was used as a negative control. All the constructs were confirmed by DNA sequencing. The shRNA-*Mettl3* (sh*Mettl3*) and negative control shRNA (shCtrl) were packaged into viruses for in vivo gene delivery by AAV helper free systems (Cell Biolabs) as previously described [34]. Briefly, AAV-293 cells were transfected with 3 plasmids: pHelper, pAAV-DJ Rep-Cap and pAAV-GFP-shRNA. Three days after transfection, cells were harvested and viruses were purified by AAV purification kit (6232, Clontech). Similarly, *METTL3* coding sequence (plasmid #53739, addgene) was cloned to the AAV vector to generate AAV-*METTL3* for overexpression and AAV-GFP was used as the control virus.

Animals were anesthetized using isoflurane and placed in a stereotaxic frame. A small incision was made to expose the skull surface and to visualize bregma and holes

were drilled in the skull overlying the dorsal hippocampus to deliver virus. One microliter virus (10^{10} infectious viral particles/mL) was stereotaxically infused bilaterally into the hippocampal at CA1 (– 2.1 mm anterior/posterior (A/P), 2.0 mm medial/lateral (M/L), 1.4 mm dorsal/ventral (D/V) from bregma) using a 10- μ L microsyringe (Hamilton). Mice were allowed to recover for 3 weeks post-surgery before further behavioral tests. For A β O treatment experiment, a guide cannula was left in place and A β O was injected bilaterally two weeks after AAV-*METTL3* infusion to the same spot [35, 36] and behavioral tests were performed two weeks later.

Behavioral tests

All behavioral tests used equal numbers of male and female mice and were conducted 3 weeks after AAV infusion, starting with Y maze spontaneous alternation task (SAT) followed by open field test, novel object recognition task and object location test. The testing chamber and Y maze were cleaned after each trial to exclude olfactory cues. All of the behavioral tests were recorded and analyzed by EthoVision XT tracking system from Noldus.

Y maze

The animals were placed in a Y-shaped maze with 3 arms of equal length that diverge at equal angles and recorded for 5 min. The total number and sequence of arm entries over the test period was scored. An arm entry occurs when all 4 limbs are within the arm and a successful spontaneous alternation was defined as consecutive entries into all 3 arms without returning to a previously visited one. The maximal number of

alternations was the total number of arm entries minus two, and the spontaneous alternation percentage was calculated as (actual alternations/maximal number of alternations) \times 100.

Open field

For open field (OF) test, mice were placed in a light opaque chamber (50 cm \times 50 cm) and recorded for 30 min. Total locomotor activity, time in center area, mean speed were automatically measured.

Object recognition tests

For novel object recognition (NOR) task, animals were placed in above chamber and allowed to explore 2 identical objects for 10 min. Two hours later, the animals were returned to the chamber with one of the two objects replaced by a novel object and the exploratory behavior was recorded for 5 min. The objects used in this study were T-25 cell culture flasks filled with sand and multicolored rectangular stacks. For object location test (OLT), spatial cues exist to help orient the mice during the training and test phases. In the training phase, two identical 50 mL falcon tubes filled with water were placed at adjacent far corners of the chamber, and mice were allowed to explore both objects in 3 blocks of 3 min each with 3-min breaks in between. Two hours later, the animals were returned to the chamber for test phase with one of the two objects displaced to adjacent empty corners, causing the 2 objects to be diagonal to each other. Mice were given 5 min to explore both objects, and the amount of time spent exploring each object was recorded. To analyze the cognitive performance, preference of novel object or displaced object was calculated as the time spent exploring the above objects divided by the cumulative time spent exploring both objects.

Immunoblot

Brain tissues or neuronal cells were lysed in 1 \times radioimmunoprecipitation assay (RIPA) buffer (9806S; Cell Signaling Technology) containing protease inhibitor mixture (5,892,791,001 and 4,906,837,001, Roche). About 30 μ g total protein extracts were resolved by SDS-PAGE and transferred to immobilon-P (IPVH00010, Millipore). After blocking with 10% nonfat milk in TBST, primary and secondary antibodies were applied and the blots were developed with Immobilon western chemiluminescent HRP substrate (WBKLS0500, Millipore). Quantification was performed using ImageJ.

Antibodies used in immunoblot were: rabbit anti-METTL3 (15073-1-AP, Proteintech), rabbit anti-METTL14 (ABE1338, Millipore), mouse anti-WTAP (60188-1-Ig, Proteintech), mouse anti-FTO (MABE227, Millipore), rabbit anti-YTHDF1 (17479-1-AP, Proteintech), rabbit anti-YTHDF2 (24744-1-AP, Proteintech), rabbit anti-YTHDF3 (25537-1-AP, Proteintech), rabbit anti-GAPDH (2118, Cell Signaling), mouse anti-AT8 (MN1020, ThermoFisher), mouse

anti-Actin (MAB1501, Millipore), mouse anti- γ H2AX (ab26350, abcam), rabbit anti-PSD-95 (3409, Cell Signaling), mouse anti-synaptophysin (MA5-11475, Invitrogen), mouse anti-caspase 9 (sc-56,076, Santa Cruz), rabbit anti-cleaved caspase 3 (9661, Cell Signaling), mouse anti-CCND1 (sc-450, Santa Cruz), mouse anti-CCND2 (Santa Cruz, sc-56,305), mouse anti-CCNB1 (sc-245, Santa Cruz). Secondary antibodies included anti-mouse/rabbit HRP-linked secondary antibody (7076/7074, CST). Primary antibodies were used at a 1:1000 dilution, with secondary antibodies used at a 1:10,000 dilution. All antibodies were validated for use in the study and detailed antibody validation profiles are available on the websites of the companies the antibodies were sourced from.

Immunostaining

Immunohistochemical and immunofluorescent analyses were performed as described previously [37]. Briefly, brain tissues from human and mice were fixed and subsequently embedded in paraffin for sectioning. Brain sections (6 μ m) were rehydrated and immunostained using primary antibodies as indicated. For immunohistochemistry, the sections were then incubated with either goat anti-mouse or goat anti-rabbit antibody, followed by species-specific peroxidase anti-peroxidase complex (Jackson, West Grove, PA, 223005024 or 323,005,024). 3-3'-Diaminobenzidine (Enzo Life Sciences, Farmingdale, NY, ACC105-0200) was used as a chromogen. All the images were acquired using Zeiss Axiovision software. For immunofluorescence, fixed neuronal cultures or rehydrated brain section were immunostained using the primary antibodies as indicated. Fluorescent secondary antibodies were subsequently applied and stained sections were imaged using Leica HyVolution SP8 confocal microscope at the CWRU SOM Light Microscopy Core Facility. Quantification was performed using ImageJ and adjacent blank area was selected as background in a region of interest for subtraction.

Antibodies used in immunostaining were: rabbit anti-METTL3 (15073-1-AP, Proteintech), rabbit anti-METTL14 (ABE1338, Millipore), mouse anti-FTO (MABE227, Millipore), rabbit anti-YTHDF1 (17479-1-AP, Proteintech), rabbit anti-m⁶A (202,003, Synaptic systems), mouse anti-m⁶A (NBP2-50525, Novus); mouse anti-AT8 (MN1020, ThermoFisher), mouse anti-NeuN (MAB377, Millipore), mouse anti-GFP (sc-9996, Santa Cruz), mouse anti- γ H2AX (ab26350, abcam), rabbit anti-4-HNE (HNE11S, Alpha Diagnostic), rabbit anti-PSD-95 (3409, Cell Signaling), mouse anti-PSD-95 (sc-32,290, Santa Cruz), mouse anti-synaptophysin (MA5-11475, Invitrogen), rabbit anti-cleaved caspase 3 (9661, Cell Signaling), rabbit anti-MAP 2 (AB5622, Chemicon), rabbit anti-GFAP (PA5-16291, Invitrogen), mouse anti-GFAP (691,102, MP Biomedicals), rabbit anti-Iba1

(PA5–21274, Thermo Fisher), mouse anti-PCNA (sc-56, Santa Cruz), mouse anti-CCND1 (sc-450, Santa Cruz), mouse anti-CCND2 (Santa Cruz, sc-56,305), mouse anti-CCNB1 (sc-245, Santa Cruz). Other secondary antibodies included Alexa Fluor 488 donkey anti-mouse secondary antibody (A21202, Invitrogen), Alexa Fluor 568 goat anti-rabbit secondary antibody (A11036, Invitrogen), Alexa Fluor 568 goat anti-mouse secondary antibody (A-11004, Invitrogen), Alexa Fluor 647 goat anti-mouse (A21235, Invitrogen), Alexa Fluor 647 goat anti-rabbit (A21245, Invitrogen). Primary antibodies were used at a 1:200 dilution, with secondary antibodies used at a 1:300 dilution.

Golgi staining

Morphological alterations in dendritic spines in mouse brains were examined by Golgi staining using FD Rapid GolgiStain™ Kit (PK401, FD NeuroTechnologies) according to the manufacturer's instructions. Spines were judged mushroom if the diameter of the head was much greater than the diameter of the neck as previously described [38].

LC-MS/MS

100 ng RNA from human frontal cortex was digested with 1 μ L nuclease S₁ from *Aspergillus oryzae* (Sigma) in 50 μ L reaction containing 10 mM NH₄OAc pH 5.3 at 42 °C for 1.5 h. Then, 1 μ L shrimp alkaline phosphatase (NEB), 3 μ L 10 x CutSmart buffer (NEB) and 1 μ L water were added and incubated at 37 °C for 1.5 h. After that, water was added to 50 μ L and the samples were filtered with the 0.22 μ m Millex Syringe filter (Millipore). 5 μ L filtered sample was injected into a C18 column (Agilent) on a UHPLC (Agilent) coupled to a SCIEX 6500+ triple quadrupole mass spectrometer in positive electrospray ionization mode. The nucleotides were quantified based on the nucleoside-to-base transition 268→136 (A), 282.1→150.1 (m⁶A), the retention time 1.26 min (A), 2.6 min (m⁶A) and compared to the calibration curves.

Reagents

Lipofectamine 2000 reagent (Invitrogen, 11,668,027) was purchased for transient transfection in neuronal cells according to the manufacturer's instructions. Rnase (AM2286, Invitrogen) and Dnase (D4513, Sigma) treatments were performed according to the manufacturer's instructions. Cresyl violet acetate (C5042, Sigma) 2.5% aqueous is used in Nissl staining of mouse brain sections. Actinomycin D (A1410, Sigma), N-Acetyl Cysteine (NAC, A7250, Sigma), flavopiridol (10,009,197, Cayman) and rhein (17,345, Cayman) were purchased and used in the treatment of primary neurons as indicated. In Situ Cell Death Detection Kit (11,684,795,910, Roche) was used to label rehydrated mouse brain sections

undergoing apoptosis following manufacturer's instructions in this study. This method is based on labeling of DNA strand breaks (TUNEL technology) and analyzed by fluorescence microscopy. After TUNEL labeling, the sections were stained for GFP using Alexa Fluor 568 goat anti-mouse secondary antibody (A-11004, Invitrogen) and FITC-labelled cells were imaged on Leica HyVolution SP8 confocal microscope.

Measurements in primary neurons

Data showing incidence of events in primary cortical neuronal cells (dendritic spine number and neurite degeneration) were obtained from multiple random regions from three independent experiments. Distal neurites of primary neurons were defined to be shortened if the neurites did not extend a 40 \times microscopic field of view as previously described [39]. Propidium iodide (P3566, Invitrogen) was added to the AAV-GFP-shRNA-infected primary neuronal cultures for 4 h before measurements in fluorescence microscopy.

Quantitative PCR analysis

To detect cellular mRNA changes in primary rat cortical neurons, RNA samples were reversely transcribed using 6-nucleotide random primers and M-MLV reverse transcriptase (M0253, NEB). Quantitative PCR reactions were performed with SYBR™ Green Master Mix (43–856-12, Applied Biosystems) and specific primers on the StepOne 96-well Real-Time PCR System (Applied Biosystems). The mRNAs levels were normalized to the GAPDH gene or 18SrRNA as indicated. The PCR reaction was performed at 95 °C for 5 min followed by 45 cycles at 95 °C for 10 s, 60 °C for 30 s. Each set of PCR reaction was performed in triplicate and CT values of each PCR reaction were obtained. The ratios of gene expression were calculated relative to the control set in the experiments. The following primer pairs were used: rat GAPDH, 5'-CAA GGA GTA AGA AAC CCT GGA C-3' (sense) and 5'-GGG ATG GAA TTG TGA GGG AGA T-3' (antisense); rat CCNA1, 5'-TGA ACA GGG GGA CAG AGA CA-3' (sense) and 5'-GAG TCA ACC AGC ATT GGG GA-3' (antisense); rat CCNB1, 5'-TCC CAC ACG GAG GAA TCT CT-3' (sense) and 5'-TCT GCA GAC GAG GTA GTC CA-3' (antisense); rat CCND1, 5'-TCA AGT GTG ACC CGG ACT G-3' (sense) and 5'-CAC TAC TTG GTG ACT CCC GC-3' (antisense); rat CCND2, 5'-GCT CTG TGT GCT ACC GAC TT -3' (sense) and 5'-GGT CCG GAT CTT CCA CAG AC -3' (antisense); rat CDKN1C 5'-GAA CGG TGC GAT CAA GAA GC -3' (sense) and 5'-ATG AAA GGT CCC AGC CGA AG -3' (antisense). Rat 18SrRNA 5'-GCT TAA TTT GAC TCA ACA CGG GA -3' (sense) and 5'-AGC TAT CAA TCT GTC AAT CCT GTC -3' (antisense).

Anti-m⁶A immunoprecipitation

Immunoprecipitation (IP) of m⁶A-modified RNA using a specific mouse anti-m⁶A (NBP2–50525, Novus) was carried out following a published protocol [40]. Briefly, total pure RNA (1.5 µg) was treated by DNase and fragmented, followed by incubation with m⁶A antibody (2 µg)-Protein G-Magnetic Beads (1.5 mg) (MJS002V2, MBL) complex in 1 × RNA IP buffer (150 mM KCl, 25 mM Tris pH 7.4, 5 mM EDTA, 0.5 mM DTT, 0.5% IGEPAL® CA-630). After extensive washing with 1 × RNA IP buffer, RNA fragments with m⁶A modification were eluted using elution buffer with free m⁶A 5' monophosphate sodium salt (NM10586, Carbosynth). Eluted RNA was used to synthesize cDNA for quantitative PCR analysis to detect the m⁶A-modified target mRNA. Same amount of fragmented pure total RNA was saved as input reference. Normal mouse IgG₁ (2 µg) (sc-3877, Santa Cruz) was used as the negative control antibody in the m⁶A IP experiment. All of the solutions were treated by RNase-secure (AM7006, Invitrogen) to irreversibly inactivate RNases. Following primers were used to detect the potential m⁶A modified regions in 3'UTR of the target genes using quantitative PCR analysis: CCND2 sense, 5'-TAG TGA GAT GCT TAC AGG A-3' and CCND2 antisense, 5'-TGC TTT GCA AAC TAC TCA TGC G-3'.

Statistical analysis

The performer(s) was (were) blinded to the experimental design in data collection and analysis. All the data represent means ± standard error of the mean (SEM). For 2 independent data comparisons, two-tailed unpaired student's t-test was used to determine statistical significance. For multiple comparisons, one-way ANOVA with bonferroni's correction was used as indicated in the text. All the statistical analyses were performed using Graphpad Prism or Excel 2016. *P*-values < 0.05 were considered significant. Data distribution was assumed to be normal, but this was not formally tested. ClinCalc was used to predetermine the minimum number sample sizes of mouse behavioral tests.

Results

Decreased neuronal m⁶A modification in AD brains

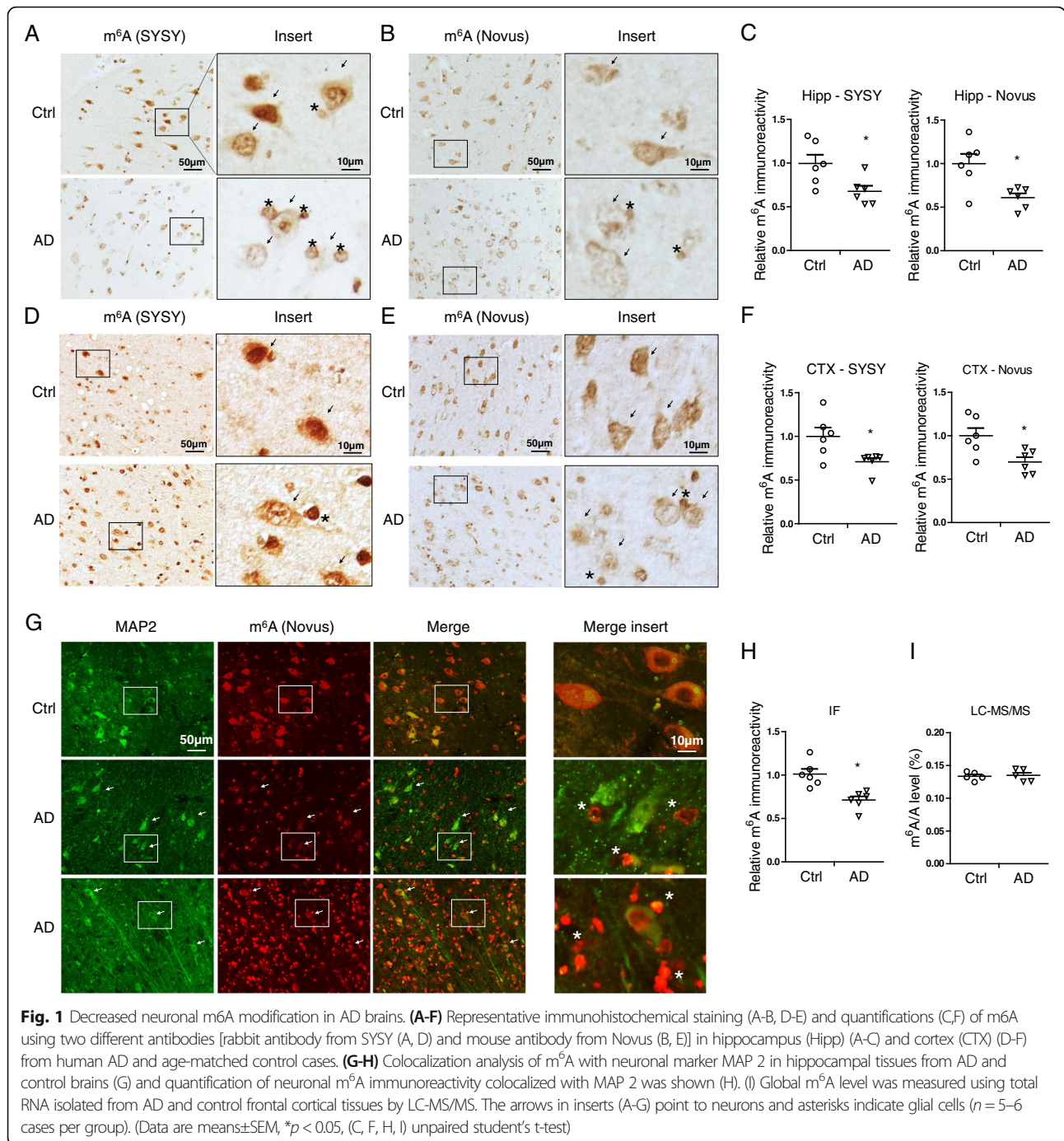
To elucidate a potential role of m⁶A modification during the course of AD, we first measured the level of m⁶A immunoreactivity in the hippocampus and cortex from AD and age-matched control patients. The immunoreactivity of m⁶A was found primarily in pyramidal neurons throughout the hippocampus (Fig. 1 A,B,C) and cortex (Fig. 1 D,E,F) of human brains using two different antibodies. Some smaller cells resembling glial cells were occasionally stained. While both DNA and RNA can have m⁶A modifications [41, 42], neuronal m⁶A immunoreactivity was only dramatically reduced after Rnase

treatment but not after Dnase treatment (Fig. S1 D), indicating that m⁶A modification predominantly exists in RNA species in human brain tissues. Comparing to m⁶A immunostaining in age-matched control brains, the RNA m⁶A modification was significantly reduced in large pyramidal neurons in the AD brain (Fig. 1 A-F). Meanwhile, it was noted that m⁶A immunoreactivity was increased in some glial-like cells surrounding the neurons in AD brain tissues (Fig. 1 A-F). No cellular structures were noted by secondary only negative controls in all of human cases from immunohistochemical and immunofluorescent analyses (Fig. S1 E-F and S2 E). Immunofluorescence co-localization study with neuronal and glial cell markers confirmed that m⁶A immunoreactivity was dramatically reduced in MAP 2-positive neurons (Fig. 1 G,H) but increased in GFAP-positive astrocytes (Fig. S1 A-C) and some iba-1 positive microglia (Fig. S1 D) in AD brains. However, the total m⁶A level was unchanged in AD brains compared with normal controls as measured by LC-MS/MS (Fig. 1 I), likely caused by differentially changed m⁶A levels in neurons and glial cells.

Decreased m⁶A-related regulator proteins in AD brains

RNA m⁶A modification is dynamically modulated by m⁶A writers and erasers and recognized by m⁶A readers [43]. Protein expression of m⁶A writers (METTL3, METTL14, and WTAP), eraser (FTO) and readers (YTHDF1, YTHDF2, and YTHDF3) in brain tissues from AD patients and age-matched control patients was determined by both immunocytochemistry and immunoblot analysis. Immunocytochemical analysis revealed extensive immunoreactivities of METTL3 and METTL14 throughout the cell body but more predominantly in the nucleus in pyramidal neurons in the hippocampus and cortex (Fig. 2 A) from elder controls. However, in AD brain, reduced immunoreactivities of METTL3 and METTL14 were noted in these neurons with a more uniform distribution between the cytosol and nucleus (Fig. 2 A,B). The m⁶A eraser FTO was observed both in cytosol and nucleus in the pyramidal neurons from controls (Fig. 2 A,B) but only background immunoreactivity of FTO was noted in these neurons from AD patients. The m⁶A reader YTHDF1 existed predominantly in the cytosol of pyramidal neurons in age-matched control brains but with reduced immunoreactivity in AD brains (Fig. 2 A,B).

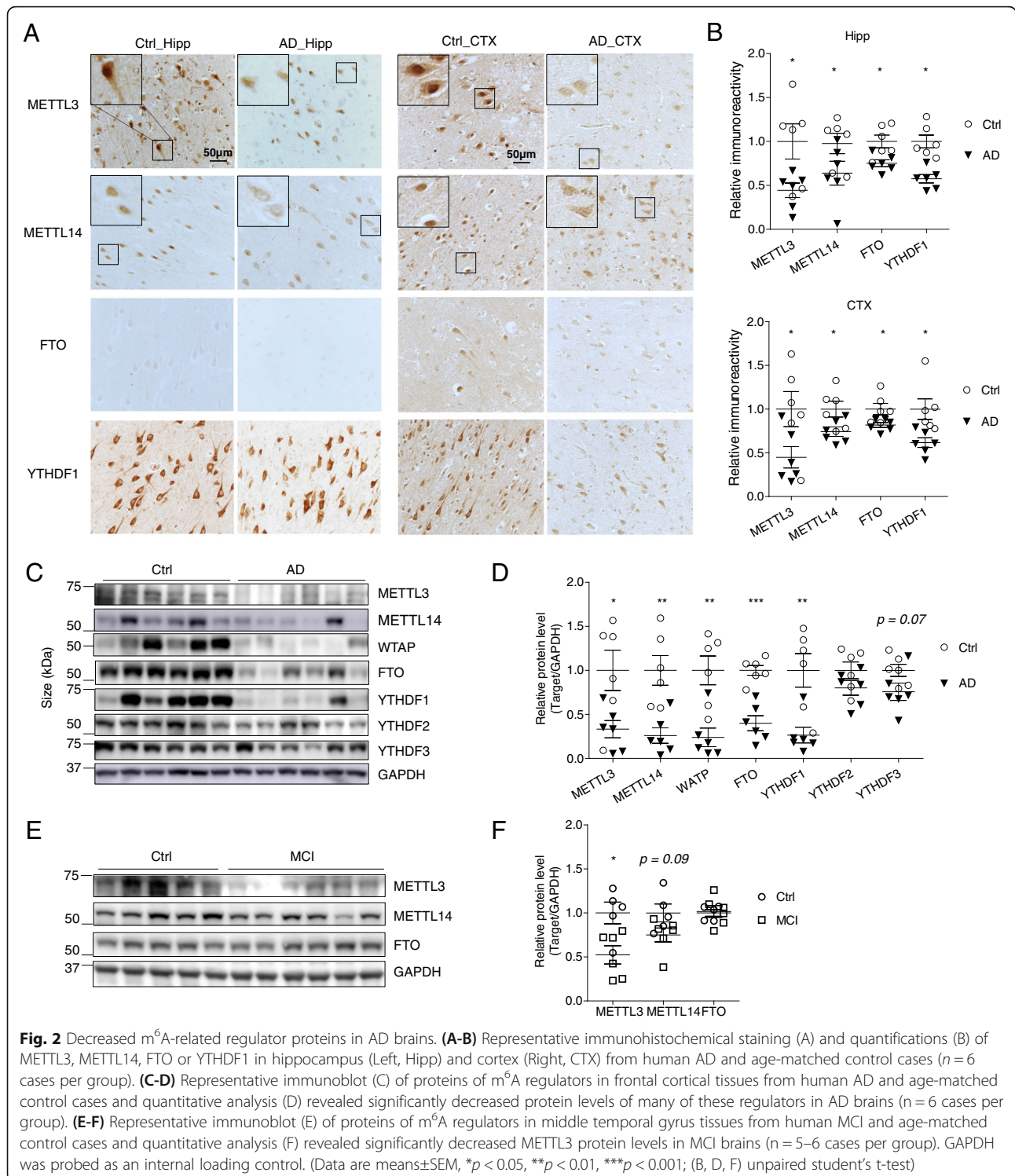
Consistently, immunoblot analysis demonstrated significant reduction in the protein levels of many of these m⁶A regulators in the brain cortical tissues from AD patients compared to that from age-matched control patients (Fig. 2 C,D): the m⁶A writers, including METTL3, METTL14 and WTAP, were significantly reduced by 66.7, 74.0, and 76.0% in AD, respectively. The eraser FTO was also significantly reduced by 60% in AD. Among the three readers measured, the level of YTHD



F1 protein was significantly reduced by 73.5% while levels of YTHDF2 or YTHDF3 proteins were reduced but did not reach significance in AD.

MCI represents the earliest symptomatic stage to AD [2, 3]. Middle temporal gyrus is one of the first temporal lobe neocortical sites affected in AD, and atrophy in middle temporal gyrus may herald the presence of future AD [44]. To investigate whether m⁶A modification plays a role in the pathogenesis of AD early in the process and METTL3 reduction likely plays a critical role.

measured the protein levels of m⁶A writers and eraser in the middle temporal gyrus from patients with MCI (Fig. 2 E). Immunoblot analysis showed that only METTL3, but not METTL14 and FTO, was significantly reduced in middle temporal gyrus from MCI patients compared with that from normal controls (Fig. 2 E,F). These data suggest that dysregulation of RNA m⁶A modification is likely involved in the pathogenesis of AD early in the process and METTL3 reduction likely plays a critical role.



Decreased neuronal METTL3 and m⁶A in the hippocampus by AAV-shMettl3

To determine the potential role of METTL3 downregulation and disturbed m⁶A regulation in neurodegeneration and pathogenesis of AD, we sought to knockdown the neuronal expression of METTL3 in vivo by using

adeno-associated virus (AAV) containing vectors co-expressing enhanced green fluorescent protein (eGFP) and METTL3-targetting shRNA (shMettl3) and determine AD-related cognitive and pathological changes. Specifically, the shMettl3 targeting sequence is located in a highly conserved region in both mouse and rat

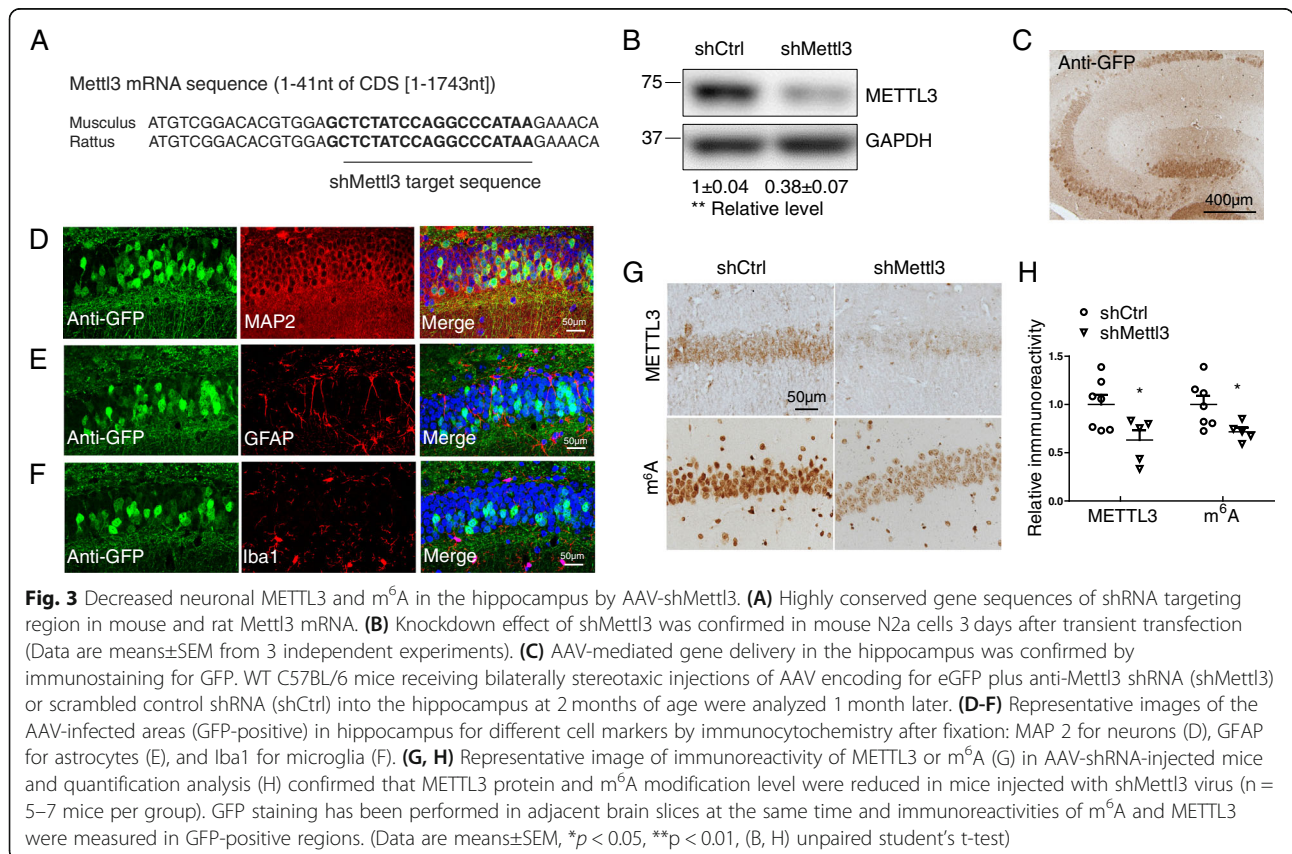
METTL3 mRNAs (Fig. 3 A), which allows efficient METTL3 knockdown in both mouse and rat neuronal cells. Significant reduction of endogenous METTL3 protein level was confirmed by western blot analysis in mouse neuroblastoma N2a cells (Fig. 3 B) and rat primary neurons (not shown) transiently transfected with AAV vector containing shMettl3 as compared to cells transfected with AAV vector containing a scramble shRNA as a negative control (shCtrl).

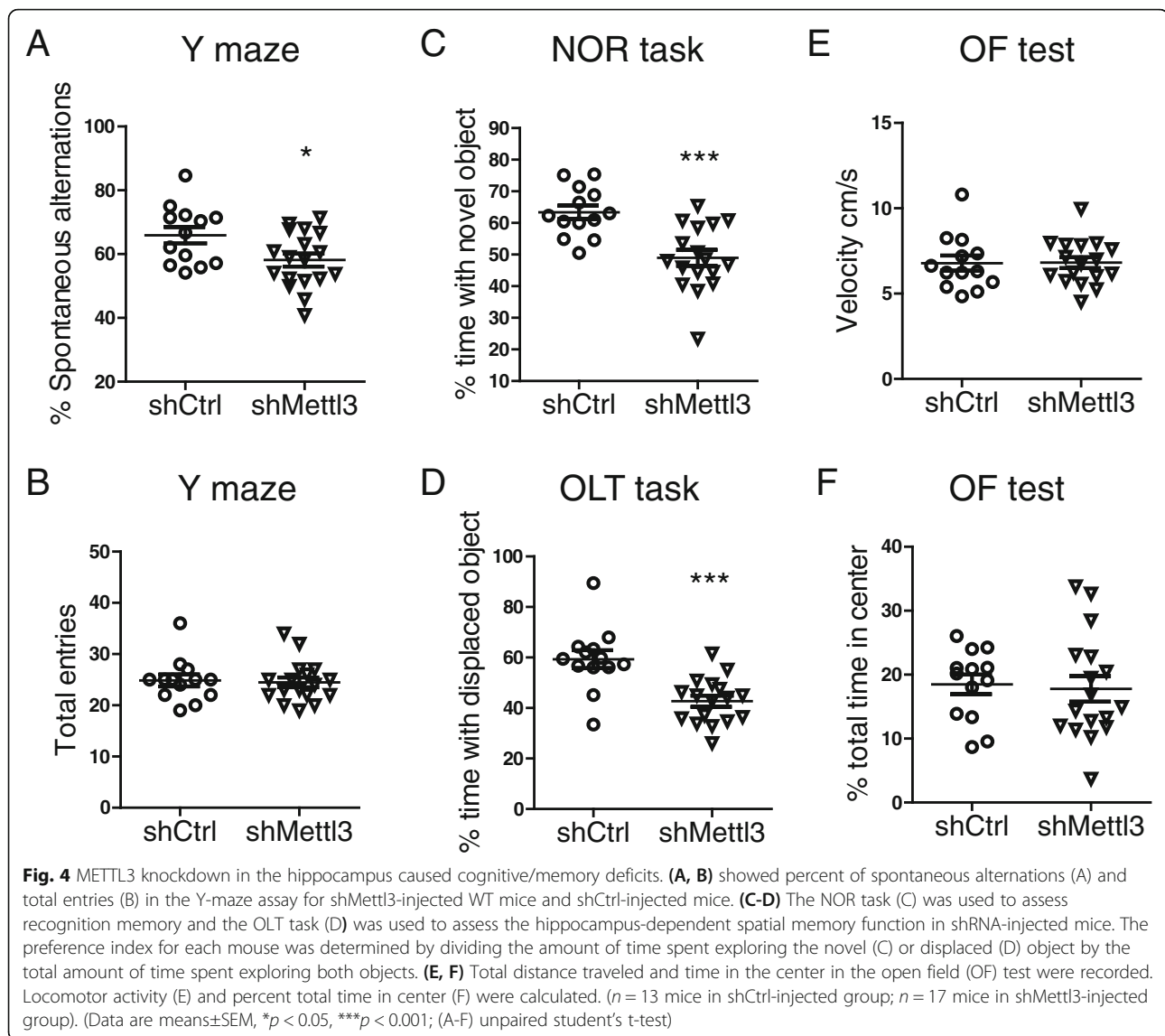
Wild type mice were bilaterally injected with AAV-GFP-shRNA (shMettl3 or shCtrl) into the hippocampal area at 9–10 weeks of age, and sacrificed and analyzed 4 weeks later. Needle tracks of intracranial injections were validated to confirm proper AAV infusion in hippocampus and no clear cell loss was noted around injection sites in all of the shCtrl mice (Fig. S3 A). Immunocytochemical analysis of GFP expression revealed GFP-positive cells mainly in the CA3 and CA1 regions in both shCtrl and shMettl3-infused mice (Fig. 3 C). Pyramidal neurons in the hippocampus were preferentially infected as confirmed by the predominant colocalization of GFP and neuronal marker MAP 2 (Fig. 3 D), but little or no colocalization of GFP and the astrocytic marker GFAP (Fig. 3 E) or the microglial marker

Iba1 (Fig. 3 F). Consequently, immunocytochemical analysis confirmed that endogenous METTL3 proteins along with neuronal m⁶A level were significantly reduced in GFP-positive pyramidal neurons of shMettl3-injected mice compared to that of shCtrl-injected mice (Fig. 3 G,H), confirming the major role of METTL3 in m⁶A modification in pyramidal neurons in the adult hippocampus.

METTL3 knockdown in the hippocampus leads to memory loss

Several behavioral tests were carried out 3 weeks after intracranial injections. In the Y-maze spontaneous alternation task (SAT), shMettl3-injected mice exhibited reduced spontaneous alternation compared to shCtrl-injected mice (Fig. 4 A), indicating an impairment in the spatial working memory caused by the knockdown of METTL3 in the hippocampus. In the novel object recognition (NOR) task to assess mouse ability to explore longer a novel object over a familiar one (Fig. 4 C), shCtrl-injected mice exhibited a 63% preference indices for the novel object as expected. In contrast, shMettl3-injected mice exhibited no differences in the exploration time between novel and familiar objects, indicating an

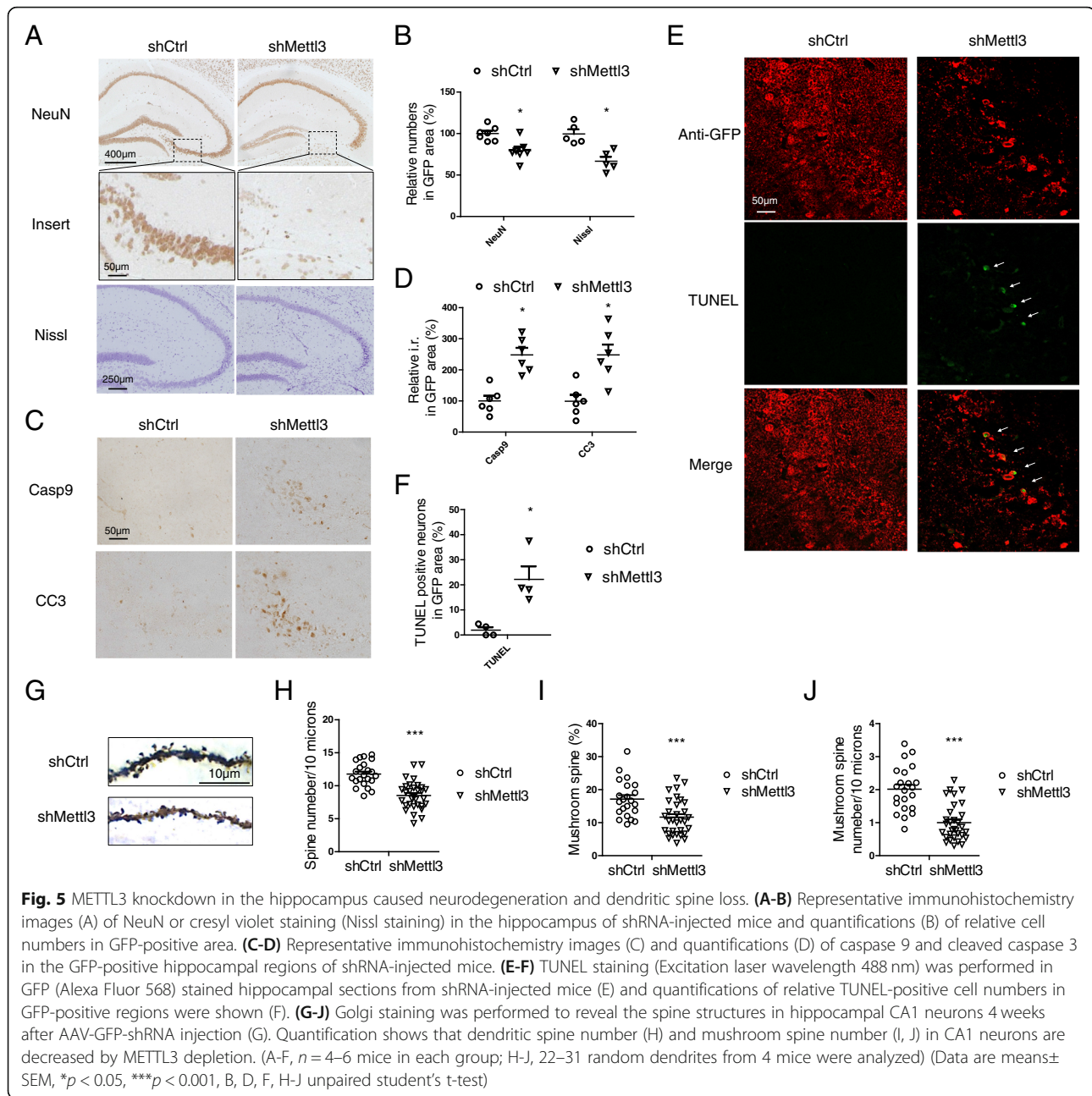




impairment in recognition memory. The hippocampus-dependent spatial memory was further evaluated using the object location test (OLT) which also revealed significantly decreased percentage of time interacting with the displaced object in shMettl3-injected mice (Fig. 4D). shMettl3 mice and shCtrl mice did not differ in the total entry number of arms during SAT test (Fig. 4B) and the amount of locomotor activity during open field (OF) test (Fig. 4E), suggesting that METTL3 reduction in the hippocampus did not affect motor performance. No anxiety-like behaviors were observed in either shCtrl mice or shMettl3 mice, as evidenced by the same amount of time spent in the center during OF test (Fig. 4F). Together, these results suggest decreased neuronal m⁶A modification in the hippocampus by METTL3 knockdown leads to cognitive deficits, the cardinal feature of AD.

METTL3 knockdown in the hippocampus causes neurodegeneration, spine loss and gliosis

AD patients suffer from extensive selective neuronal loss in the hippocampal areas [45, 46]. Interestingly, dramatic neuronal loss was found in the hippocampus of shMettl3-injected mice compared with that of shCtrl-injected mice as evidenced by the significant loss of NeuN-positive neurons. This was further confirmed by the significant loss of Nissl-stained cells (Fig. 5A,B). Caspase 3 is a key mediator of neuronal programmed cell death and its activation is a feature of many neurodegenerative diseases [47, 48]. Indeed, increased immunoreactivities of activated/cleaved caspase 3 and its upstream activator, caspase 9, were found in the hippocampus of shMettl3-injected mice as compared to that of shCtrl-injected mice (Fig. 5C,D). TUNEL staining also revealed the appearance of apoptotic cells in the hippocampal



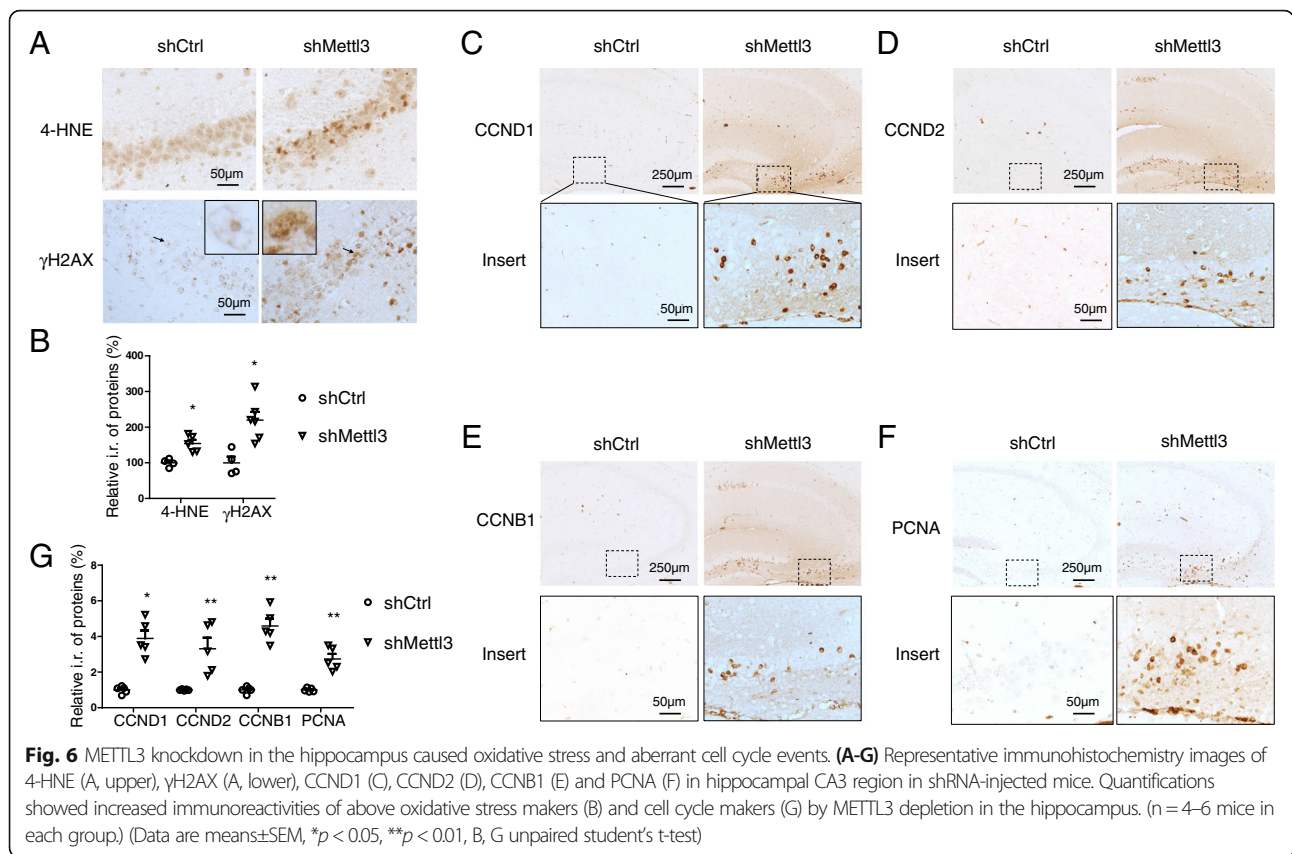
region of the shMettl3-injected mice but not in the shCtrl-injected mice (Fig. 5 E,F). To assess neuronal deficits, Golgi staining was performed to investigate synaptic changes (Fig. 5 G). Significantly decreased number of dendritic spines (Fig. 5 G,H) and stable mushroom spines (Fig. 5 G,I,J) were found in the pyramidal neurons in the hippocampus of shMettl3-injected mice which likely underlies cognitive deficits in these mice.

In addition to neuronal deficits, increased activation of microglia (Fig. S3 B,C) detected by iba-1 immunostaining and increased activation of astrocytes (Fig. S3 D,E) detected by GFAP staining were also found in the

hippocampus of shMettl3-infected mice compared with shCtrl-injected mice. Considering that AAV-shRNA only infected neurons in the hippocampus (Fig. 3 D-F), the increased microgliosis and astrocytosis is likely a response to neuronal damage.

METTL3 knockdown in the hippocampus causes oxidative stress and aberrant cell cycle events

Extensive oxidative stress features the vulnerable regions of the brain affected by AD and it is considered to be critical to AD pathogenesis [49]. The immunoreactivity of 4-hydroxy-2-trans-nonenal (HNE), an oxidative stress



marker, was significantly increased in the hippocampus of shMettl3-injected mice (Fig. 6 A,B). Continuous attack of DNA by reactive oxygen species (ROS) leads to DNA damages such as strand breaks [50]. Consistently, increased DNA damage, as demonstrated by significantly increased immunoreactivity of γ -H2AX (Fig. 6 A,B), was also found in the hippocampus of shMettl3-injected mice.

Aberrant cell cycle activation is a critical component of the DNA damage response in postmitotic neurons [51]. Unexpected neuronal death can be induced by aberrant cell cycle events in postmitotic neurons in the central nerve system [52] which is believed to be involved in neuronal loss in AD [53, 54]. Interestingly, increased immunoreactivity of cyclin-D1 (CCND1), cyclin-D2 (CCND2) and cyclin B1 (CCNB1) was found in pyramidal neurons in the hippocampus by METTL3 depletion, but none of these cyclins were observed in shCtrl mice (Fig. 6 C-E, G). Abnormal expression of proliferating cell nuclear antigen (PCNA), one of the cell cycle proteins, was reported to predict the sites of neuronal cell death in AD brains [55] and animal models of neurodegeneration [56, 57]. PCNA-positive cells were also found in the hippocampus of shMettl3-injected mice, but not in shCtrl-injected mice (Fig. 6 F,G). Our data suggest that METTL3 knockdown causes increased oxidative stress and aberrant cell cycle

events, which could be involved in METTL3 knockdown-induced neuronal death.

METTL3 knockdown induces dysregulation of cell cycle genes and apoptotic changes in primary neuronal cultures

To determine the relationship between METTL3 knockdown-induced aberrant cell cycle events and neurodegeneration, we investigated cell cycle changes in primary neurons after METTL3 knockdown in vitro. Transfection of shMettl3 effectively reduced endogenous METTL3 protein level (Fig. S4 A,B) and m⁶A immunoreactivity in rat primary neurons (Fig. 7 A,B). Analysis of expression level of multiple cyclin genes assessed by quantitative PCR analysis (Fig. 7 C) revealed that METTL3 knockdown led to significantly elevated mRNA levels of CCND1 and CCND2 in primary neurons. Interestingly, cyclin dependent kinase inhibitor 1C (CDKN1C) was dramatically decreased by METTL3 knockdown (Fig. 7 C). It is worth noting that CCND2 was identified as a m⁶A target in the mouse brain [58] and we also verified by m⁶A-immunoprecipitation (IP) assay that m⁶A antibody pulled down about 12% of total input CCND2 mRNA by quantitative PCR (Fig. 7 D). To examine whether increased gene expression was caused by changes in m⁶A-mediated RNA decay, we measured the life time of CCND2 mRNA by inhibition of gene transcription with actinomycin D in primary cortical neurons. After actinomycin D

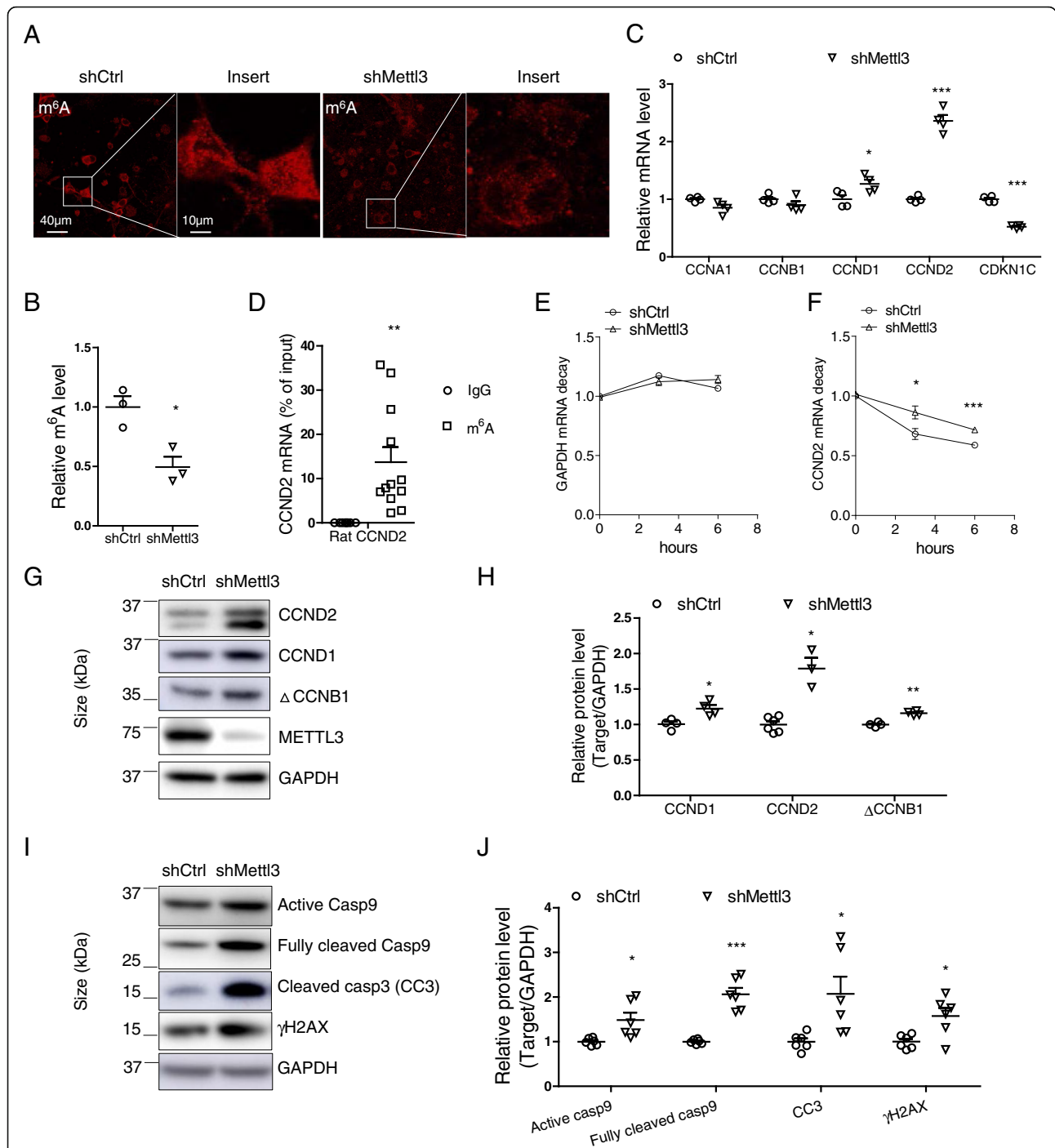


Fig. 7 METTL3 knockdown induced dysregulation of cell cycle genes and apoptotic changes in primary neuronal cultures. **(A, B)** Representative immunofluorescence image (A) and quantification analysis of m⁶A immunoreactivity (B) in primary cortical neurons after AAV-GFP-shRNA infection revealed significantly decreased neuronal m⁶A modification by METTL3 depletion. **(C)** Quantitative PCR analysis of cell cycle genes in primary neurons after Mettl3 knockdown mediated by AAV-shRNA infection. GAPDH was used as a reference gene for quantitative gene expression analysis. **(D)** Total pure RNA from adult rat cortical tissue was immunoprecipitated with a specific m⁶A antibody (Novus) or a mouse IgG control. CCND2 mRNAs were pulled down and detected by quantitative PCR. **(E–J)** Primary rat cortical neurons from E16–18 embryos were infected with AAV-GFP-shMettl3 or AAV-GFP-shCtrl on DIV 7. Six days after AAV injection, neurons were treated with actinomycin D (5 µg/ml). Representative mRNA profiles of GAPDH (E) and CCND2 (F) at 0-, 3-, and 6-h time points after treatment were shown. 18S rRNA was used as reference for quantitative analysis. **(G–J)** Eight to nine days after AAV infection, neuron extracts were used for immunoblot analysis (G, I) and quantification of protein changes were shown (H, J) (Data are means±SEM from at least 3 independent experiments, *p < 0.05, **p < 0.01, ***p < 0.001; B–F, H, J unpaired student’s t-test)

treatment, GAPDH mRNA level was not apparently affected in either shCtrl neurons or shMettl3 neurons at 3 and 6 h (Fig. 7 E). However, CCND2 mRNA level was declined by 32 and 41% in shCtrl neurons at 3 and 6 h after treatment, respectively. In the contrary, CCND2 mRNA was declined by only 14 and 28% in shMettl3 neurons (Fig. 7 F). Our data indicated mRNA level of CCND2 in shCtrl neurons declined more rapidly than in shMettl3 neurons after inhibition of gene transcription. Thus, the increased level of m⁶A-modified CCND2 by the depletion of METTL3 was likely caused by delayed mRNA clearance. Consistent with mRNA changes, immunoblot analysis revealed that the protein levels of CCND1 and CCND2 were significantly increased in primary neurons by shMettl3 (Fig. 7 G,H). Interestingly, METTL3 depletion caused significant increase in ~35 kDa protein product of CCNB1 (Δ CCNB1) (Fig. 7 G,H), a caspase-dependent cleavage product during mitotic catastrophe sufficient to induce mitotic block and apoptosis [59]. Indeed, Caspase-9/3 apoptotic pathway was activated as evidenced by increased active/cleaved caspases and increased DNA damage response was also detected as indicated by increased γ H2AX after METTL3 treatment in these primary neurons (Fig. 7 I,J).

METTL3 knockdown causes postsynaptic deficit and neurite degeneration in primary neuronal culture

Dendritic spines as defined by protrusions of 0.5–5 μ m in length with a clear neck and mushroom-like heads or a stubby shape [31] (Fig. 8 A) were examined by GFP fluorescence. Markedly reduced spine density was observed in primary neurons with METTL3 knockdown compared with control neurons (Fig. 8 A,B). Consistently, immunofluorescence analysis (Fig. 8 E,F) revealed reduced immunoreactivity of postsynaptic density protein 95 (PSD95). Interestingly, no changes in the immunoreactivity of presynaptic protein synaptophysin (Syp) was noted in primary neurons after METTL3 knockdown. Immunoblot analysis (Fig. 8 C,D) confirmed significantly reduced protein expression of PSD95 but not synaptophysin in primary neurons after METTL3 knockdown.

The existence of shortened or fragmented distal neurites was considered as a sign of neurite degeneration [39]. We observed an increase in the percentage of neurons with degenerative neurites in shMettl3-transfected primary neurons (Fig. S4 A,C). Meanwhile, the neurite number per soma was significantly reduced by METTL3 knockdown (Fig. S4 A,D). Similarly, immunofluorescence analysis revealed significant decrease in the protein level of dendritic marker MAP 2 in neurons after METTL3 knockdown (Fig. 8 G,H).

Inhibition of oxidative stress and cell cycle events alleviates shMettl3-induced cell cycle abnormalities and neurodegenerative changes in primary neurons

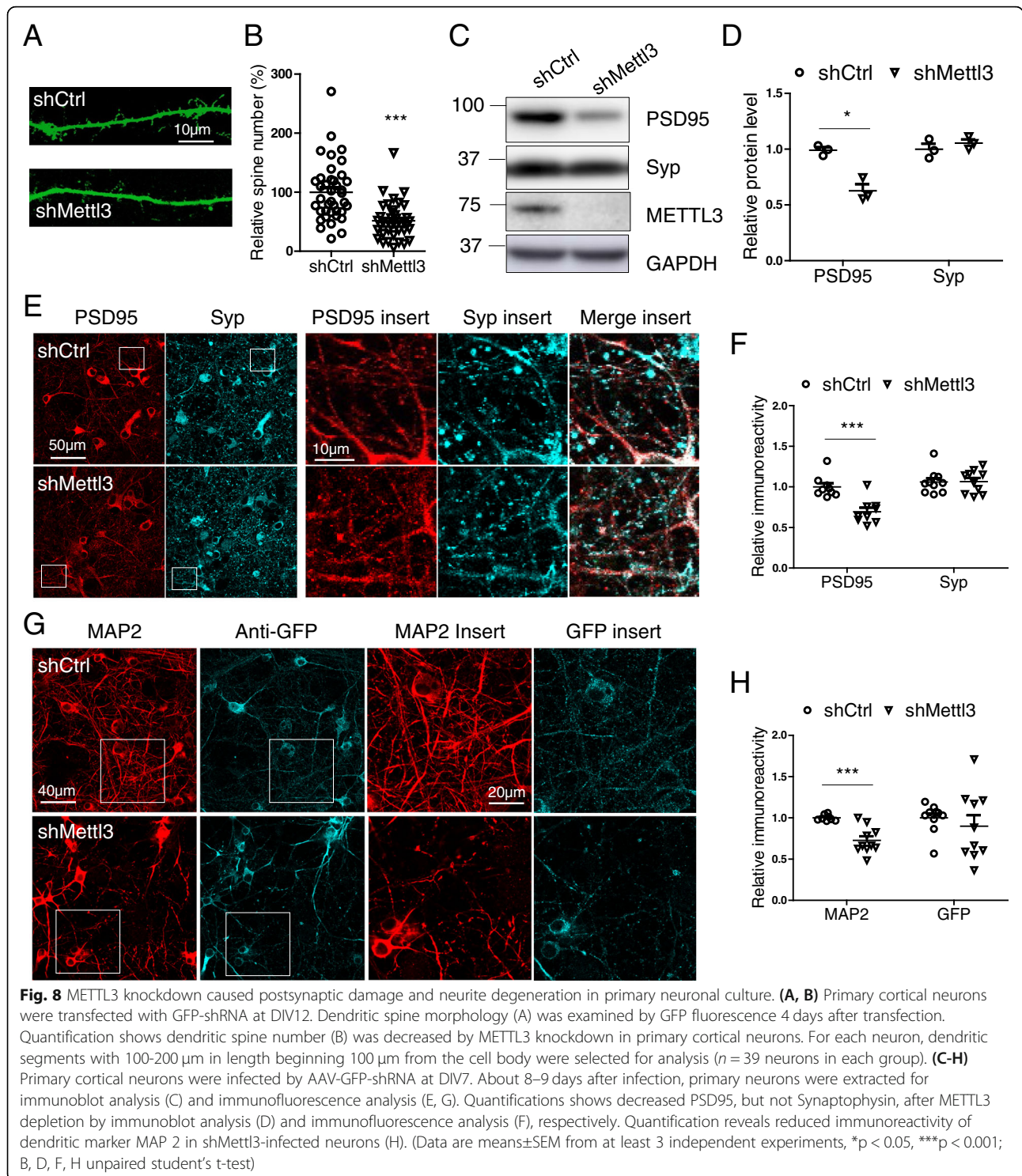
To explore the causal relationship between METTL3 knockdown-induced oxidative stress, aberrant cell cycle events and degenerative changes in neurons, we used antioxidant N-acetyl cysteine (NAC) or cell cycle inhibitor flavopiridol to treat shMettl3-infected primary neurons. Flavopiridol treatment almost completely prevented METTL3 knockdown-induced abnormal increase in the protein levels of CCND1, CCND2 and Δ CCNB1, suggesting effective inhibition of METTL3 knockdown-induced aberrant cell cycle events (Fig. 9 A–D). Importantly, in this condition, METTL3 knockdown-induced caspase 3 (Fig. 9 A,E) activation and other neurodegenerative changes such as loss of postsynaptic PSD95 (Fig. 9 F,G), dendritic MAP 2 (Fig. 9 F,H) were also significantly inhibited. Interestingly, NAC also alleviated METTL3 knockdown-induced aberrant cell cycle events and caspase 3 activation (Fig. 9 A–E) along with restoration of postsynaptic PSD95 (Fig. 9 F,G) and dendritic MAP 2 (Fig. 9 F,H) in treated primary neurons. METTL3 knockdown-induced neuronal death, as indicated by propidium iodide (PI) uptake, was also alleviated by NAC and flavopiridol treatment (Fig. 9 I).

Inhibition of m⁶A demethylation reduces shMettl3-induced deficits in primary neurons

Next we investigated whether restoration of m⁶A modification by treatment of rhein, a natural product and small-molecule inhibitor of FTO demethylase [60], could rescue METTL3 depletion-induced reduced m⁶A modification and neuronal deficits. As reported previously [61], basal levels of neuronal m⁶A modification was elevated by rhein treatment (Fig. 10 A). METTL3 knockdown-induced m⁶A decrease in neurons was blocked by rhein treatment (Fig. 10 B). Interestingly, inhibition of m⁶A demethylation effectively alleviated dysregulation of cell cycle genes (i.e., CCND 1 and 2) and the cleavage/activation of caspase 3 induced by METTL3 knockdown in primary neurons (Fig. 10 C–F). METTL3 knockdown-induced other degenerative changes such as loss of postsynaptic PSD95 (Fig. 10 G,H) and dendritic MAP 2 (Fig. 10 G,I) were also restored by rhein. METTL3 knockdown-induced neuronal loss was also partially rescued by rhein treatment as measured by PI uptake assay (Fig. 10 J).

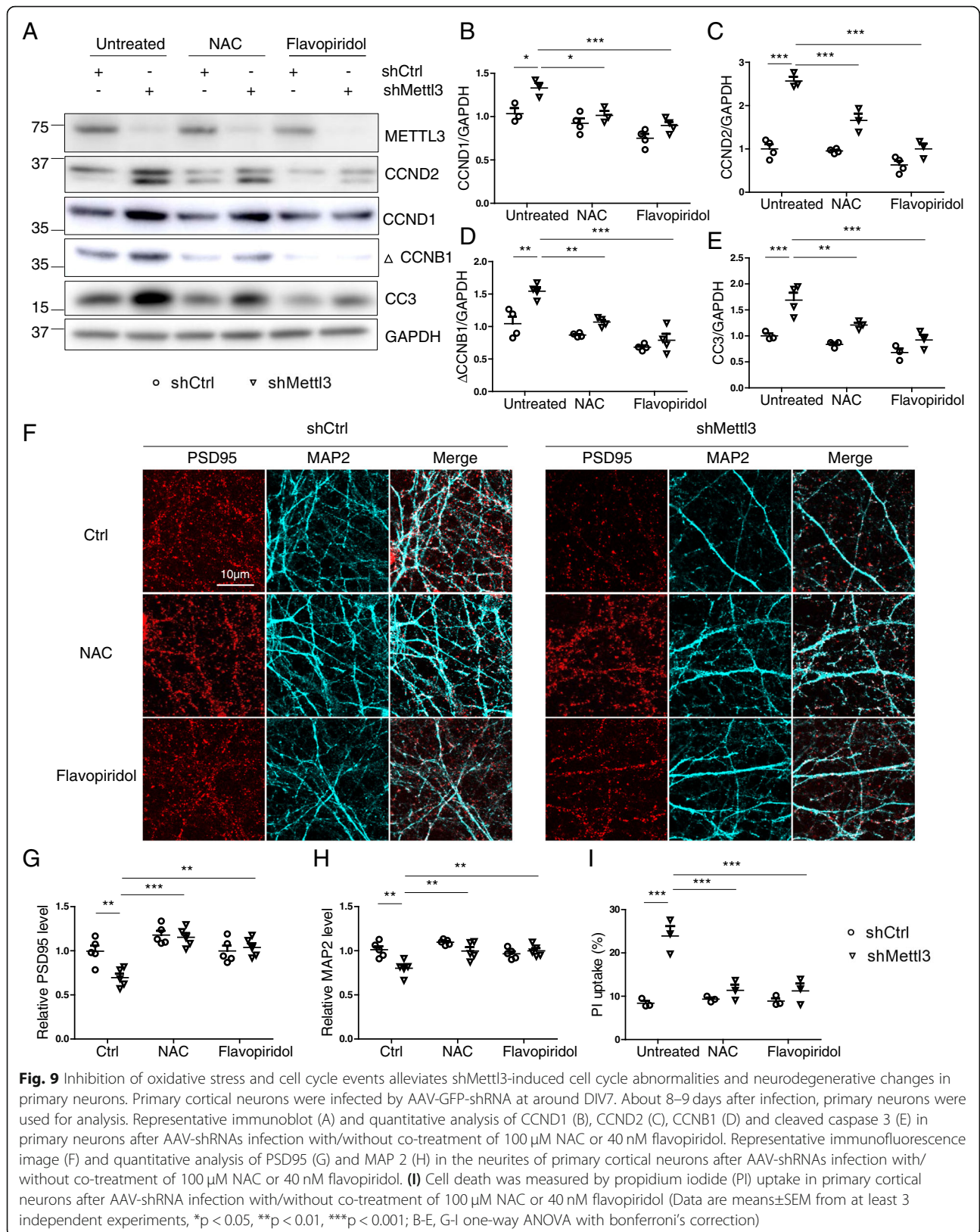
METTL3 overexpression rescues A β -induced synaptic toxicity both in vitro and in vivo

It was suggested that soluble A β oligomers (A β O) are the culprit of AD which cause synaptic loss and neuronal dysfunction in AD [62]. Interestingly, A β O treatment caused significantly reduced METTL3 expression



in rat primary cortical neurons (Fig. 11 A,B). To assess how METTL3 expression impacts A β -induced synaptic deficits, METTL3 expression was manipulated in primary cortical neurons which were then treated with 2.5 μM A β Os for 3 days. As previously reported, immunoblot analysis demonstrated that A β Os treatment led

to significant reduction of PSD95 protein level in shCtrl-infected neurons, which was dramatically exacerbated by METTL3 knockdown (Fig.11 C,D). This was corroborated by immunostaining analysis which also revealed that A β Os-induced PSD95 reduction in shCtrl-infected neurons was further exacerbated by METTL3



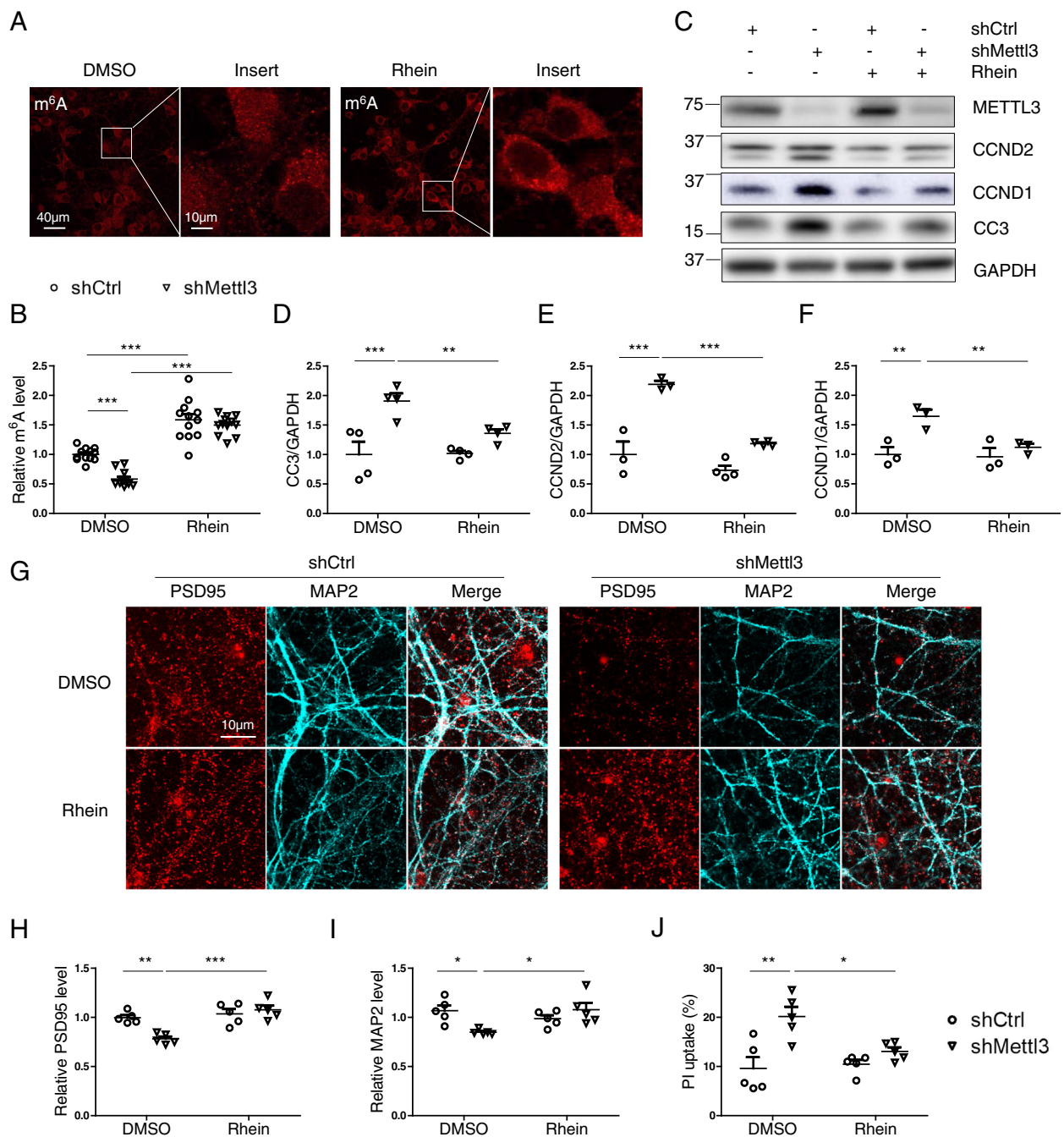
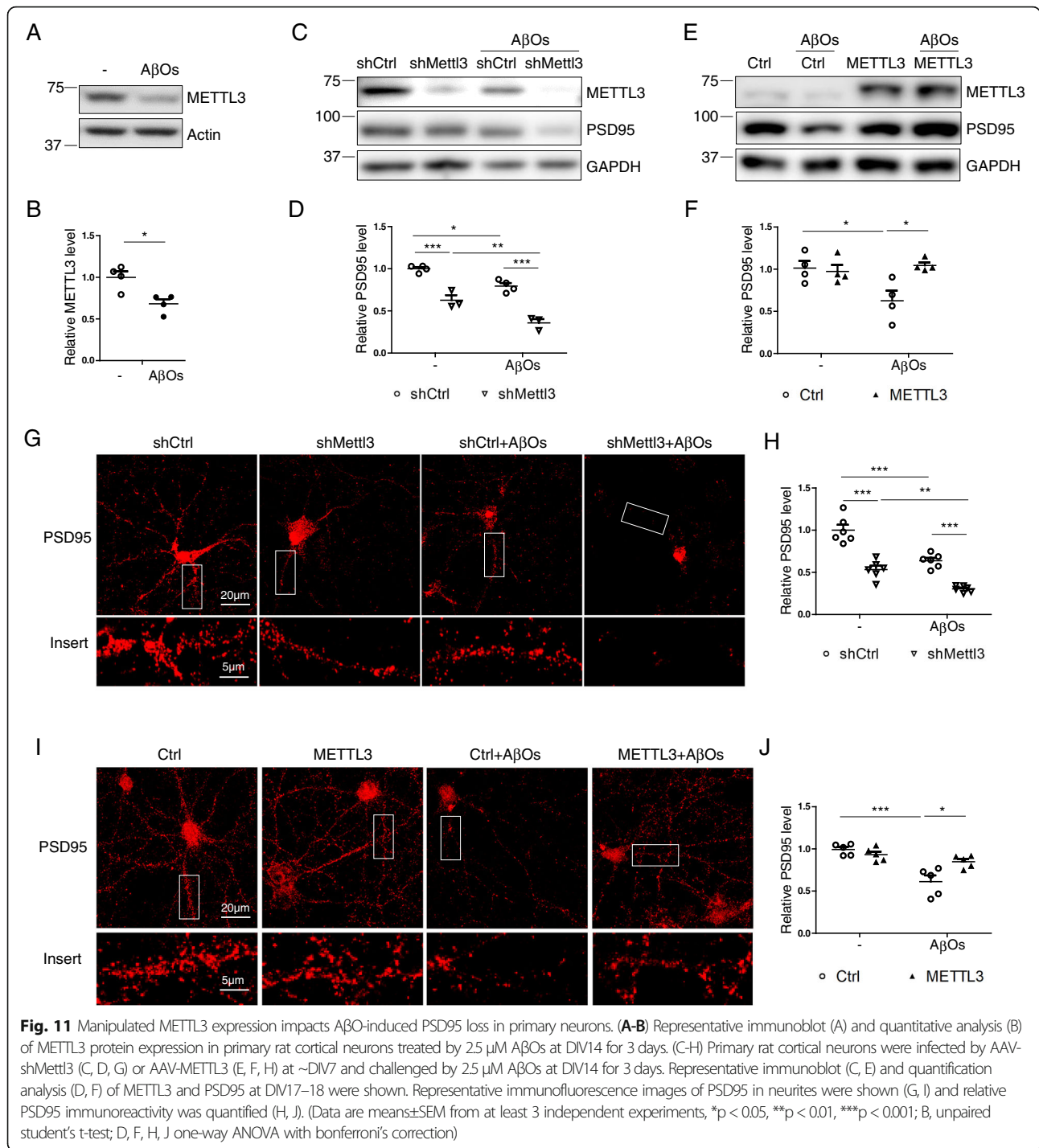


Fig. 10 Inhibition of m⁶A demethylation reduces shMettl3-induced deficits in primary neurons. Primary cortical neurons were infected by AAV-GFP-shRNA at around DIV7. About 8–9 days after infection, primary neurons were used for analysis. Representative immunofluorescence image (A) and quantitative analysis of m⁶A (B) in the primary cortical neurons after AAV-shRNAs infection with/without co-treatment of 0.25 μM rhein (inhibitor for m⁶A demethylation) for 24 h. (C–I) Representative immunoblot (C) and quantitative analysis of cleaved caspase 3 (D), CCND2 (E) and CCND1 (F) in primary neurons after AAV-shRNAs infection with/without co-treatment of 0.25 μM rhein. (n = 3 in each group). Representative immunofluorescence image (G) and quantitative analysis of PSD95 (H) and MAP2 (I) in the neurites of primary cortical neurons after AAV-shRNAs infection with/without co-treatment of Rhein. (J) Cell death was measured by propidium iodide (PI) uptake in primary cortical neurons after AAV-shRNA infection with/without co-treatment of Rhein (Data are means ± SEM from at least 3 independent experiments, *p < 0.05, **p < 0.01, ***p < 0.001; B, D–F, H–J one-way ANOVA with bonferroni's correction)



knockdown (Fig. 11 G,H). On the contrary, METTL3 overexpression significantly alleviates AβOs-induced PSD95 reduction by both immunoblot analysis (Fig. 11 E,F) and immunofluorescence analysis (Fig. 11 I,J).

To assess whether METTL3 overexpression rescues AβOs-induced synaptic damage and cognition/memory deficits in vivo, we stereotactically injected AAV-METTL3 into the CA1 region of 9–10 week old C57BL/

6 mice (Fig.S6 A,B) and AβOs were injected into the same site two weeks later. After an additional two weeks, these mice were subject to cognitive tests before sacrifice. As we reported previously [35, 36], AβOs treatment led to significant cognitive deficits as determined by Y-maze task (Fig. 12 A,B), novel object recognition test (Fig. 12 C) and object location test (Fig. 12 D). Importantly, METTL3 overexpression effectively rescued the

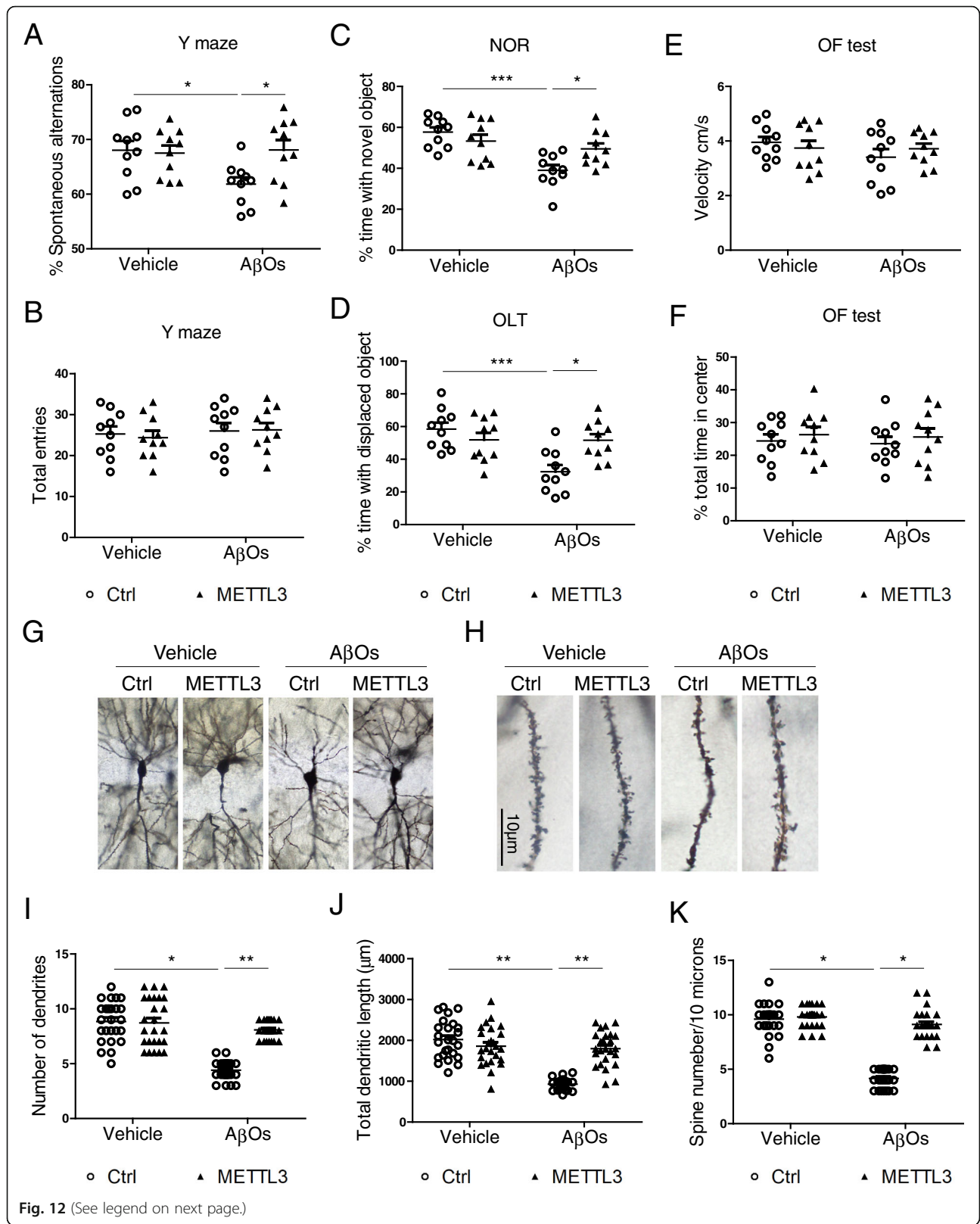


Fig. 12 (See legend on next page.)

(See figure on previous page.)

Fig. 12 METTL3 overexpression rescues A β O-induced cognitive impairment and synaptic deficits in vivo. WT C57BL/6 mice receiving bilaterally stereotaxic injections of AAV-METTL3/AAV-Ctrl into the hippocampus at ~ 2 months of age were administrated with A β O preparations 2 weeks later. Behavioral tests were performed 2 week after A β O treatment. Cognitive functions were measured by Y maze task (A-B), novel object recognition test (NOR) (C) and object location test (OLT) (D). Locomotor function (E) and exploring activity (F) were measured by open field test (OF) ($n = 10$ mice/group, sex matched). **(G-K)** Dendrites (G) and spines (H) in the infused hippocampal areas were examined by Golgi stain. Number of dendrites (I), total length of dendrites (J) and number of dendritic spines (K) were measured. ($n = 25$ neurons from 5 mice in each group) (* $p < 0.05$, ** $p < 0.01$, *** $p < 0.001$; A-F, I-K, one-way ANOVA with bonferroni's correction)

A β O-induced cognitive deficits in these mice. Locomotor function (Fig. 12 E) and exploring activities (Fig. 12 F) were unaffected by A β O and METTL3 as indicated by open field tests. Consistently, golgi staining revealed that A β O-induced loss of dendrites and spines in the hippocampus was almost completely prevented in METTL3 overexpression mice (Fig. 12 G-K).

Discussion

Despite relatively high RNA m⁶A level in the brain [58], study of m⁶A modification in the brain is a nascent field, and the significance of this epigenetic mark in brain development and neuronal function is just beginning to be appreciated. In this study, we found significantly reduced RNA m⁶A modification in the susceptible pyramidal neurons but increased RNA m⁶A in glial cells in the hippocampus and cortex of AD patients. Significantly reduced protein expression of m⁶A writers (METTL3, METTL14 and WTAP), eraser (FTO) and reader (YTHDF1) accompanied by reduced nuclear distribution of METTL3/14 in the pyramidal neurons were also found in AD brain. While these findings in human AD brain are correlational, it helps establish the pathophysiological relevance of the study into METTL3 dysregulation in AD. Importantly, METTL3 and METTL14 levels were reduced in the brain of MCI patients, a prodromal stage of AD, suggesting an early role of dysregulated RNA m⁶A modification during the course of AD. AD is characterized by cognitive impairment and progressive neurodegeneration, which is believed to be caused by early synaptic damage and eventually selective neuronal loss in AD-affected brain areas [63]. Signifying the critical role of the appropriate m⁶A equilibrium in the hippocampal function in adult mice, reduced m⁶A deposition induced by METTL3 knockdown in the hippocampus of adult mice caused significant cognitive/memory impairment. In exploring the brain pathology that underlie the abnormal memory decline after METTL3 knockdown, we found significant dendritic spine and synaptic abnormalities and extensive neuronal death in the hippocampus, all features of AD. These abnormal neuronal deficits and death are probably specific effects of reduced overall m⁶A modification since they could be rescued in primary neurons by treatment of rhein, a small-molecule inhibitor of FTO demethylase

that restored m⁶A modification levels. Additional experiments demonstrated that treatment of A β oligomers caused reduced METTL3 expression in primary neurons and overexpression of METTL3 rescued A β oligomers-induced synaptic deficits both in vitro and in vivo. More importantly, overexpression of METTL3 rescued A β oligomers-induced cognitive deficits in adult mice.

A major finding of this study is significantly reduced neuronal RNA m⁶A modification along with significantly reduced expression of m⁶A regulators such as METTL3 in AD brain. The finding of significantly reduced METTL3 expression in MCI patients underscores an early and critical role of m⁶A dysregulation in AD pathogenesis. The lack of changes in other m⁶A regulators during MCI phase suggests that METTL3 reduction may be an initiating factor in m⁶A dysregulation which lead to reduction in other m⁶A regulators at a later stage during the course of AD because METTL3 and METTL14 form a heterodimeric methyltransferase complex and METTL3 knockdown leads to METTL14 reduction [64]. Similarly, changes in other m⁶A regulators, especially m⁶A erasers such as FTO reduction could be an adaptive response to early changes in METTL3 and/or 14. These will need to be investigated in future studies into the role of m⁶A dysregulation in the pathogenesis of AD. Nevertheless, our finding of reduced METTL3 expression in AD is consistent with the recent report of reduced METTL3 expression in AD based on the expression profile study using a public RNA-seq dataset [65] which suggested accumulation of METTL3 in the insoluble fraction may play a role. Our study further suggested that abnormal redistribution of m⁶A-related proteins between nucleus and cytosol may also contribute to the decrease of neuronal m⁶A modification in AD. A nuclear anchoring protein ZC3H13 in RNA m⁶A methylation complex was identified recently [66], highlighting that nuclear localization of m⁶A regulatory complex is critical for m⁶A modification and its biological function. In this regard, more dramatic reduction of METTL3 and METTL14 writers in the nucleus was noted in AD neurons. Consistent with reduced METTL3 in AD brain, we found treatment of A β oligomers caused reduced METTL3 expression in primary neurons. However, it remains elusive how m⁶A modification and METTL3 expression change in the brain of APP

transgenic models because conflicting results were reported: Han et al. reported increased global m⁶A levels in total RNA in the cortex and hippocampus of APP/PS1 mice at 9 months of age using an m⁶A RNA methylation quantification kit [67]. They also reported an increased mRNA expression of METTL3 in these mice [67]. On the contrary, a more recent study demonstrated significantly reduced METTL3 expression along with reduced m⁶A levels in poly(A) mRNA in 6 months old 5xFAD mice measured by LC-MS/MS [68]. It remains to be determined what caused this discrepancy which could be due to different sample preparation (total RNA vs. mRNA) and/or methods (antibody based colorimetric method vs. LC-MS/MS). Model-specific effects may also be involved since neuronal death was only observed in the 5xFAD model.

Another major finding is that METTL3 knockdown caused cognitive deficits and neurodegeneration which support a critical role of METTL3 reduction in mediating major deficits related to AD. This was further strengthened by the findings that METTL3 overexpression fully rescued A β oligomers-induced synaptic deficits and cognitive deficits in vivo. We also observed other neuronal abnormalities related to AD pathogenesis by shMettl3-induced m⁶A dysregulation in the adult hippocampus, which could shed light on the underlying neurodegeneration mechanism. Pyramidal neurons are postmitotic and quiescent cells. However, aberrant cell cycle events, likely induced by increased DNA damage, has long been noted as a prominent feature in many of the susceptible pyramidal neurons which is considered to result in their eventual demise through apoptosis and contribute to the degeneration of neuronal tissue in AD [53, 69]. Most recently, integration of epigenetic and transcriptomic data demonstrates a pro-apoptotic reactivation of the cell cycle in post-mitotic AD neurons [6]. In this study, we found METTL3 knockdown caused increased oxidative stress and DNA damage, aberrant cell cycle events and apoptotic activation in pyramidal neurons in the adult hippocampus in vivo after METTL3 knockdown. While a causal relationship between these abnormal changes (oxidative stress and aberrant cell cycle events) and eventual cell death remains to be established in vivo since the possibility that these abnormal changes could simply be due to the degenerative changes of neurons during death has not been ruled out, shMettl3-induced dysregulation of cell cycle genes was rescued by restoration of m⁶A after rhein treatment, accompanied by blocked activation of apoptosis and neuronal deficits in vitro. It highlights that METTL3 depletion reduces m⁶A modification and thus induces dysregulation of cell cycle genes, activation of apoptotic pathway and AD-related neuronal deficits. Moreover, inhibition of cell cycle events by flavopiridol treatment

alleviates shMettl3-induced dysregulation of cell cycle genes and neuronal deficits and apoptosis, indicating a causative role of dysregulation of cell cycle genes in shMettl3-induced AD-related neuronal deficits and death. How do pyramidal neurons commit to an unscheduled cell cycle after METTL3 knockdown that lead to their doomed fate? It has been shown that there is an enrichment of genes in m⁶A-tagged transcripts related to the cell cycle, stem cells and neuronal differentiation and m⁶A methylation of mRNAs related to the cell cycle regulates their turnover and changes the temporal specification and cell cycle progression [24, 70]. We also confirmed m⁶A methylation in the G1 phase regulator CCND2 and increased levels of mRNA and protein of CCND2 in the hippocampus or primary neurons after METTL3 knockdown. It is possible that reduced m⁶A deposition after METTL3 knockdown leads to uncoordinated changes in the expression of cell cycle regulators including CCND1/2 and resulted in unscheduled cell cycle re-entry that leads to apoptosis. Our data also suggested that oxidative stress may contribute to aberrant cell cycle-induced neuronal apoptosis since antioxidant NAC alleviates shMettl3-induced dysregulation of cell cycle genes and protects against the subsequent apoptosis activation and neuronal damage. In this regard, it is noted that cell cycle and oxidative stress can be team players in neurodegenerative disorders and oxidative stress can lead to cell cycle abnormalities through DNA damage response [71]. Interestingly, RNA m⁶A methylation regulates the ultraviolet-induced DNA damage response [64], indicating the protective role of RNA m⁶A modification in DNA repair. Therefore, it is possible that the accumulation of DNA damage as evidenced by γ H2AX due to increased oxidative stress and a lack of proper DNA repair after METTL3 knockdown also contributes to the unscheduled cell cycle re-entry in these susceptible pyramidal neurons.

Contrary to significantly reduced neuronal RNA m⁶A modification in the hippocampus and cortex of AD patients, significantly increased RNA m⁶A modification was noted in the microglia and astrocytes in these brain areas. This probably explains the lack of changes in the overall levels of m⁶A deposition in AD brain measured by LC-MS/MS. It is unclear what caused differential RNA m⁶A deposition between neurons and glial cells in AD. Its functional significance is also not clear. Inflammation occurs in pathologically vulnerable regions of the AD brain and contributes to AD pathogenesis as demonstrated in animal models and clinical studies [72]. Activated microglia and astrocytes were found in the hippocampus after METTL3 knockdown. However, since only neuronal cells were infected by AAV shRNA in our mouse model, enhanced inflammation in the mouse hippocampus after METTL3 knockdown was

probably a pathological response to shMettl3-induced synaptic damage and cell death instead of being the direct effect of reduced glial m⁶A. Therefore, it is still possible that increased m⁶A deposition in glial cells could contribute to the enhanced inflammation and disease development which should be further explored.

There are methodological limitations to this study. First, m⁶A antibodies can cross-react with N⁶, 2'-O-dimethyladenosine (m⁶Am), a modification found adjacent to the N⁷-methylguanosine (m⁷G) cap at the first nucleotide of certain mRNAs [73]. However, the pathological roles of neuronal METTL3 reduction and RNA m⁶A dysregulation in AD are unlikely affected by this limitation, since a cap-specific adenosine methyltransferase (CAPAM) is responsible for m⁶Am modification [74]. The effect of m⁶Am modification on m⁶A measurement is unknown in this study and potential function of m⁶Am modification in AD needs further exploration. Second, cell-type specific changes of m⁶A in AD were only demonstrated by immunocytochemistry which depends on the specificity of the antibody. This should be confirmed by different methods with large number of human samples. However, it's technically difficult to prepare intact neurons in sufficient amount from postmortem human brains for m⁶A measurement by LC-MS/MS. Lastly, the *in vitro* and *in vivo* models used in the current study involved acute treatment of AβOs. It would be of interest to determine the impact of METTL3 in aged mouse models carrying either mutant APP or tau.

Conclusion

Overall, our study demonstrated that RNA m⁶A modification has an essential role in maintaining synaptic structure and neuronal survival and function in adult neurons in the hippocampus, which has broader implication in brain health. More specifically, we demonstrated that the m⁶A-related epitranscriptomic dysregulation contributes to the neurodegeneration and pathogenesis of AD, which opens new avenues of investigation into the pathophysiological function of m⁶A in the neurodegenerative diseases and how it becomes dysregulated during AD. Our study also suggested that METTL3-mediated m⁶A dysregulation may be a therapeutic target for AD.

Abbreviations

AAV: adeno-associated virus; AD: Alzheimer's disease; ALKBH5: α-ketoglutarate-dependent dioxygenase alkB homolog 5; CCNB1: cyclin B1; CCND1: cyclin-D1; CCND2: cyclin-D2; CDKN1C: cyclin dependent kinase inhibitor 1C; CWRU: Case Western Reserve University; eGFP: enhanced green fluorescent protein; FTO: fat mass and obesity associated protein; IP: immunoprecipitation; m⁶A: N⁶-methyladenosine; MCI: mild cognitive impairment; METTL3: methyltransferase like 3; NAC: N-acetyl cysteine; NOR: novel object recognition; OF: open field; OLT: object location test; PCNA: proliferating cell nuclear antigen; PI: propidium iodide; PSD95: postsynaptic density protein 95; RIPA: radioimmunoprecipitation

assay; ROS: reactive oxygen species; SAT: spontaneous alternation task; SEM: standard error of the mean; shCtrl: scramble shRNA as a negative control; shMettl3: METTL3-targeting shRNA; Syp: synaptophysin; WTAP: Wilms Tumor 1 Associated Protein

Supplementary Information

The online version contains supplementary material available at <https://doi.org/10.1186/s13024-021-00484-x>.

Additional file 1: Supplementary Fig. 1. Characterizations of AD brain tissues and negative controls for immunostaining of m⁶A modifications and its regulators in brain tissues. (A-C) Representative images of pTau (AT8) immunohistochemistry (A) and immunoblot analysis (B) in AD. Hyper phosphorylated Tau exists in all of the AD hippocampal cases (A) and significantly elevated pTau (AT8) protein level was noted in quantitative analysis (C). (D) Normal human hippocampal sections were treated with RNase or DNase overnight before stained for m⁶A using rabbit m⁶A antibody (SYSY, synaptic systems). Immunoreactivities of m⁶A modification were decreased in hippocampal tissue after RNase treatment, indicating m⁶A modifications exist in RNA. No change in m⁶A immunoreactivity was observed in hippocampal tissue after DNase treatment. Negative control experiments were performed without primary antibody during RNase and DNase treatment and no cellular structure was noted. (E-F) Negative control experiments were performed without primary antibody in immunostaining for m⁶A modification (E) and m⁶A regulators in human AD and control brain cases. (n = 6, *p < 0.05, B, unpaired student's t-test).

Additional file 2: Supplementary Fig. 2. m⁶A is increased in astrocytes in AD hippocampus, but limited colocalization of m⁶A with Iba1 in AD was observed. (A-B) Colocalization of m⁶A (Novus, A; SYSY, B) with astrocyte marker GFAP (ThermoFisher, A; MP Biomedicals, B) in hippocampal tissues from AD and control brains. (C) Quantification revealed that m⁶A immunoreactivity was increased in astrocytes in AD hippocampal tissues compared with control. (D) AD and control hippocampal sections were stained for m⁶A (Novus) and Iba1. Only some colocalization of m⁶A and Iba1 was observed in AD and control hippocampal sections. (E) Negative control experiments were performed without primary antibody in immunostaining for m⁶A modification in human brain cases (n = 5–6 in each group, *p < 0.5, C, unpaired student's t-test).

Additional file 3: Supplementary Fig. 3. Validation of intracranial injection into hippocampus by needle track and induced neuroinflammation by METTL3 depletion in mouse hippocampus. (A) A representative image of needle track (arrow) of AAV-injected mice was shown. GFP immunoreactivity was detected in area adjacent to the needle track. NeuN staining revealed severe neuronal loss around injected areas only in AAV-shMettl3 injected mice but not AAV-shCtrl injected mice. (B-E) Representative images of immunohistochemistry for Iba1 (B) and GFAP (ThermoFisher, D) in hippocampal CA1/2 or CA3 areas in shRNA-injected mice and their quantification (C for astrocyte and E for microglia) analysis showed that METTL3 knockdown caused neuroinflammation in mouse hippocampus. (n = 4–7, *p < 0.5, **p < 0.01; C, E, unpaired student's t-test).

Additional file 4: Supplementary Fig. 4. METTL3 depletion leads to neurite degeneration in primary neurons. (A-D) GFP-shRNA was transfected into primary cortical neurons at DIV 9–12 using Lipofectamine 2000 according to manufacturer's instruction. Then neuronal cultures were used in following analysis 4 days after transfection. Representative images of immunofluorescence for METTL3 (A) and quantification of METTL3 immunoreactivity (B) in positively-transfected (GFP) neurons showed that GFP-shMettl3 transfection efficiently knockdown the endogenous METTL3 in neurons (n = 11–15 neurons). Analysis of neuronal morphology based on GFP fluorescence showed increased percentage of neurons with abnormal neurites (C) and decreased neurite numbers per neuron (D) in METTL3 depleted neurons (n = 183–210 neurons). (*p < 0.5, **p < 0.01; B-D, unpaired student's t-test).

Additional file 5: Supplementary Fig. 5. Statistical analysis of relative changes in protein levels between shMettl3 and shCtrl groups (i.e.,

shMettl3/shCtrl ratio) in response to NAC, Flavopiridol or Rhein based on data presented in Fig. 9 and Fig. 10. (A-D) shMettl3-induced significant elevations of CCND2, ⁴CCNB1 and CC3 (i.e., shMettl3/shCtrl ratio significantly greater than 1) or reduction of PSD95 and MAP 2 (shMettl3/shCtrl ratio significantly less than 1) are rescued by NAC, Flavopiridol or Rhein treatment. (*p < 0.5, **p < 0.01; A-D, unpaired student's t-test).

Additional file 6: Supplementary Fig. 6. Validation of AAV-mediated METTL3 overexpression in mouse hippocampus. GFP expression of AAV-ctrl (A) was detected by fluorescence in hippocampal area and (B) METTL3 overexpression was confirmed by western blot in AAV-METTL3 mouse hippocampus.

Acknowledgments

We thank Drs. Jiong Shi and Thomas G. Beach of Banner Sun Health Research Institute for providing brain tissues from MCI patients and controls.

Authors' contributions

Conceptualization and design of experiments, X.Z. and F.Z.; Performance of Experiments and collection of data, F.Z., S.G. and K.P.; Methodology, X.Z., Y.X., F.Z., S.G., L.Q., Q.A., S.S., W.W.; Data interpretation: X.Z., Y.X., F.Z., B.T., Q.D. and C.H.; Writing of manuscript, X.Z. and F.Z.; Manuscript Discussion, X.Z., Y.X., F.Z., B.T., S.S., W. W., Q.D. and C.H.

Funding

This work was supported by National Institute of Health (NS083498 and AG049479 to X. Z.). The work of W.W. was in part supported by the National Institute of Aging P30 AG062428 01 grant as a Program Participant of the Research Education Component (REC) of the Cleveland Alzheimer's Disease Research Center (CADRC).

Availability of data and materials

All the data supporting the conclusions of the current study are presented in the figures and they are available from the corresponding authors upon reasonable request. There are no restrictions on data availability. Source data are provided with this paper.

Declarations

Ethics approval and consent to participate

Not applicable.

Consent for publication

Not applicable.

Competing interests

The authors declare that they have no competing interests.

Author details

¹Department of Pathology, Case Western Reserve University, 2103 Cornell Road, Cleveland, OH 44106, USA. ²Department of Pharmaceutical Sciences, School of Pharmacy and Pharmaceutical Sciences, University at Buffalo, the State University of New York, Buffalo, NY 14214, USA. ³Department of Neurology, Xiangya Hospital, Central South University, Changsha, Hunan, China. ⁴Department of Chemistry, The University of Chicago, Chicago, IL, USA. ⁵Department of Biochemistry and Molecular Biology, Howard Hughes Medical Institute, The University of Chicago, Chicago, IL, USA.

Received: 21 June 2021 Accepted: 13 August 2021

Published online: 30 September 2021

References

- Alzheimer's A. 2016 Alzheimer's disease facts and figures. *Alzheimers Dement.* 2016;12(4):459–509. <https://doi.org/10.1016/j.jalz.2016.03.001>.
- Morris JC, Cummings J. Mild cognitive impairment (MCI) represents early-stage Alzheimer's disease. *J Alzheimers Dis.* 2005;7(3):235–9; discussion 255–262. <https://doi.org/10.3233/JAD-2005-7306>.
- Morris JC, Storandt M, Miller JP, McKeel DW, Price JL, Rubin EH, et al. Mild cognitive impairment represents early-stage Alzheimer disease. *Arch Neurol.* 2001;58(3):397–405. <https://doi.org/10.1001/archneur.58.3.397>.
- Guo T, Zhang D, Zeng Y, Huang TY, Xu H, Zhao Y. Molecular and cellular mechanisms underlying the pathogenesis of Alzheimer's disease. *Mol Neurodegener.* 2020;15(1):40. <https://doi.org/10.1186/s13024-020-00391-7>.
- Lord J, Cruchaga C. The epigenetic landscape of Alzheimer's disease. *Nat Neurosci.* 2014;17(9):1138–40. <https://doi.org/10.1038/nn.3792>.
- Li P, Marshall L, Oh G, Jakubowski JL, Groot D, He Y, et al. Epigenetic dysregulation of enhancers in neurons is associated with Alzheimer's disease pathology and cognitive symptoms. *Nat Commun.* 2019;10(1):2246. <https://doi.org/10.1038/s41467-019-10101-7>.
- Frye M, Harada BT, Behm M, He C. RNA modifications modulate gene expression during development. *Science.* 2018;361(6409):1346–9. <https://doi.org/10.1126/science.aau1646>.
- Huang H, Weng H, Chen J. The biogenesis and precise control of RNA m(6) a methylation. *Trends Genet.* 2020;36(1):44–52. <https://doi.org/10.1016/j.tig.2019.10.011>.
- Zaccara S, Ries RJ, Jaffrey SR. Reading, writing and erasing mRNA methylation. *Nat Rev Mol Cell Biol.* 2019;20(10):608–24. <https://doi.org/10.1038/s41580-019-0168-5>.
- Shi H, Wei J, He C. Where, when, and how: context-dependent functions of RNA methylation writers, readers, and erasers. *Mol Cell.* 2019;74(4):640–50. <https://doi.org/10.1016/j.molcel.2019.04.025>.
- Bokar JA, Shambaugh ME, Polayes D, Matera AG, Rottman FM. Purification and cDNA cloning of the AdoMet-binding subunit of the human mRNA (N6-adenosine)-methyltransferase. *RNA.* 1997;3(11):1233–47.
- Schwartz S, Mumbach MR, Jovanovic M, Wang T, Maciag K, Bushkin GG, et al. Perturbation of m6A writers reveals two distinct classes of mRNA methylation at internal and 5' sites. *Cell Rep.* 2014;4(1):284–96. <https://doi.org/10.1016/j.celrep.2014.05.048>.
- Liu J, Yue Y, Han D, Wang X, Fu Y, Zhang L, et al. A METTL3-METTL14 complex mediates mammalian nuclear RNA N6-adenosine methylation. *Nat Chem Biol.* 2014;10(2):93–5. <https://doi.org/10.1038/nchembio.1432>.
- Ping XL, Sun BF, Wang L, Xiao W, Yang X, Wang WJ, et al. Mammalian WTAP is a regulatory subunit of the RNA N6-methyladenosine methyltransferase. *Cell Res.* 2014;24(2):177–89. <https://doi.org/10.1038/cr.2014.3>.
- Agarwala SD, Blitzblau HG, Hochwagen A, Fink GR. RNA methylation by the MIS complex regulates a cell fate decision in yeast. *PLoS Genet.* 2012;8(6):e1002732. <https://doi.org/10.1371/journal.pgen.1002732>.
- Jia G, Fu Y, Zhao X, Dai Q, Zheng G, Yang Y, et al. N6-methyladenosine in nuclear RNA is a major substrate of the obesity-associated FTO. *Nat Chem Biol.* 2011;7(12):885–7. <https://doi.org/10.1038/nchembio.687>.
- Zheng G, Dahl JA, Niu Y, Fedorcsak P, Huang CM, Li CJ, et al. ALKBH5 is a mammalian RNA demethylase that impacts RNA metabolism and mouse fertility. *Mol Cell.* 2013;49(1):18–29. <https://doi.org/10.1016/j.molcel.2012.10.015>.
- Meyer KD, Jaffrey SR. Rethinking m(6) a readers, writers, and erasers. *Annu Rev Cell Dev Biol.* 2017;33(1):319–42. <https://doi.org/10.1146/annurev-cellbio-100616-060758>.
- Wang X, Zhao BS, Roundtree IA, Lu Z, Han D, Ma H, et al. N(6)-methyladenosine modulates messenger RNA translation efficiency. *Cell.* 2015;161(6):1388–99. <https://doi.org/10.1016/j.cell.2015.05.014>.
- Wang X, Lu Z, Gomez A, Hon GC, Yue Y, Han D, et al. N6-methyladenosine-dependent regulation of messenger RNA stability. *Nature.* 2014;505(7481):117–20. <https://doi.org/10.1038/nature12730>.
- Li A, Chen YS, Ping XL, Yang X, Xiao W, Yang Y, et al. Cytoplasmic m(6) a reader YTHDF3 promotes mRNA translation. *Cell Res.* 2017;27(3):444–7. <https://doi.org/10.1038/cr.2017.10>.
- Shi H, Wang X, Lu Z, Zhao BS, Ma H, Hsu PJ, et al. YTHDF3 facilitates translation and decay of N(6)-methyladenosine-modified RNA. *Cell Res.* 2017;27(3):315–28. <https://doi.org/10.1038/cr.2017.15>.
- Engel M, Eggert C, Kaplick PM, Eder M, Roh S, Tietze L, et al. The role of m(6)a/m-RNA methylation in stress response regulation. *Neuron.* 2018;99(2):389–403 e389. <https://doi.org/10.1016/j.neuron.2018.07.009>.
- Yoon KJ, Ringeling FR, Vissers C, Jacob F, Pokrass M, Jimenez-Cyrus D, et al. Temporal control of mammalian cortical neurogenesis by m(6) a methylation. *Cell.* 2017;171(4):877–89 e817. <https://doi.org/10.1016/j.cell.2017.09.003>.
- Weng YL, Wang X, An R, Cassin J, Vissers C, Liu Y, et al. Epitranscriptomic m(6) a regulation of axon regeneration in the adult mammalian nervous system. *Neuron.* 2018;97(2):313–25 e316. <https://doi.org/10.1016/j.neuron.2017.12.036>.

26. Merkurjev D, Hong WT, Iida K, Oomoto I, Goldie BJ, Yamaguti H, et al. Synaptic N(6)-methyladenosine (m(6)a) epitranscriptome reveals functional partitioning of localized transcripts. *Nat Neurosci*. 2018;21(7):1004–14. <https://doi.org/10.1038/s41593-018-0173-6>.
27. Widagdo J, Zhao QY, Kempen MJ, Tan MC, Ratnu VS, Wei W, et al. Experience-dependent accumulation of N6-Methyladenosine in the prefrontal cortex is associated with memory processes in mice. *J Neurosci*. 2016;36(25):6771–7. <https://doi.org/10.1523/JNEUROSCI.4053-15.2016>.
28. Walters BJ, Mercaldo V, Gillon CJ, Yip M, Neve RL, Boyce FM, et al. The role of the RNA demethylase FTO (fat mass and obesity-associated) and mRNA methylation in hippocampal memory formation. *Neuropsychopharmacology*. 2017;42(7):1502–10. <https://doi.org/10.1038/npp.2017.31>.
29. Shi H, Zhang X, Weng YL, Lu Z, Liu Y, Lu Z, et al. m(6) a facilitates hippocampus-dependent learning and memory through YTHDF1. *Nature*. 2018;563(7730):249–53. <https://doi.org/10.1038/s41586-018-0666-1>.
30. Zhang Z, Wang M, Xie D, Huang Z, Zhang L, Yang Y, et al. METTL3-mediated N(6)-methyladenosine mRNA modification enhances long-term memory consolidation. *Cell Res*. 2018;28(11):1050–61. <https://doi.org/10.1038/s41422-018-0092-9>.
31. Wang X, Su B, Lee HG, Li X, Perry G, Smith MA, et al. Impaired balance of mitochondrial fission and fusion in Alzheimer's disease. *J Neurosci*. 2009;29(28):9090–103. <https://doi.org/10.1523/JNEUROSCI.1357-09.2009>.
32. Khachaturian ZS. Diagnosis of Alzheimer's disease. *Arch Neurol*. 1985;42(11):1097–105. <https://doi.org/10.1001/archneur.1985.04060100083029>.
33. Mirra SS, Heyman A, McKeel D, Sumi SM, Crain BJ, Brownlee LM, et al. The consortium to establish a registry for Alzheimer's disease (CERAD). Part II. Standardization of the neuropathologic assessment of Alzheimer's disease. *Neurology*. 1991;41(4):479–86. <https://doi.org/10.1212/WNL.41.4.479>.
34. Wang W, Yin J, Ma X, Zhao F, Siedlak SL, Wang Z, et al. Inhibition of mitochondrial fragmentation protects against Alzheimer's disease in rodent model. *Hum Mol Genet*. 2017;26(21):4118–31. <https://doi.org/10.1093/hmg/ddx299>.
35. Xu Y, Zhu N, Xu W, Ye H, Liu K, Wu F, et al. Inhibition of Phosphodiesterase-4 reverses Abeta-induced memory impairment by regulation of HPA Axis related cAMP signaling. *Front Aging Neurosci*. 2018;10:204. <https://doi.org/10.3389/fnagi.2018.00204>.
36. Cui SY, Yang MX, Zhang YH, Zheng V, Zhang HT, Gurney ME, et al. Protection from amyloid beta peptide-induced memory, biochemical, and morphological deficits by a phosphodiesterase-4D allosteric inhibitor. *J Pharmacol Exp Ther*. 2019;371(2):250–9. <https://doi.org/10.1124/jpet.119.259986>.
37. Zhao F, Wang W, Wang C, Siedlak SL, Fujioka H, Tang B, et al. Mfn2 protects dopaminergic neurons exposed to paraquat both in vitro and in vivo: implications for idiopathic Parkinson's disease. *Biochim Biophys Acta*. 2017;1863(6):1359–70. <https://doi.org/10.1016/j.bbdis.2017.02.016>.
38. Harris KM, Jensen FE, Tsao B. Three-dimensional structure of dendritic spines and synapses in rat hippocampus (CA1) at postnatal day 15 and adult ages: implications for the maturation of synaptic physiology and long-term potentiation. *J Neurosci*. 1992;12(7):2685–705. <https://doi.org/10.1523/JNEUROSCI.12-07-02685.1992>.
39. Irobi J, Almeida-Souza L, Asselbergh B, De Winter V, Goethals S, Dierick I, et al. Mutant HSPB8 causes motor neuron-specific neurite degeneration. *Hum Mol Genet*. 2010;19(16):3254–65. <https://doi.org/10.1093/hmg/ddq234>.
40. Dominissini D, Moshitch-Moshkovitz S, Salmon-Divon M, Amariglio N, Rechavi G. Transcriptome-wide mapping of N(6)-methyladenosine by m(6)A-seq based on immunocapturing and massively parallel sequencing. *Nat Protoc*. 2013;8(1):176–89. <https://doi.org/10.1038/nprot.2012.148>.
41. Xiao CL, Zhu S, He M, Chen ZQ, Chen Y, Yu G, et al. N(6)-Methyladenine DNA modification in the human genome. *Mol Cell*. 2018;71(2):306–18 e307. <https://doi.org/10.1016/j.molcel.2018.06.015>.
42. Wu TP, Wang T, Seetin MG, Lai Y, Zhu S, Lin K, et al. DNA methylation on N(6)-adenine in mammalian embryonic stem cells. *Nature*. 2016;532(7599):329–33. <https://doi.org/10.1038/nature17640>.
43. Yang Y, Hsu PJ, Chen YS, Yang YG. Dynamic transcriptomic m(6) a decoration: writers, erasers, readers and functions in RNA metabolism. *Cell Res*. 2018;28(6):616–24. <https://doi.org/10.1038/s41422-018-0040-8>.
44. Convit A, de Asis J, de Leon MJ, Tarshish CY, De Santi S, Rusinek H. Atrophy of the medial occipitotemporal, inferior, and middle temporal gyri in nondemented elderly predict decline to Alzheimer's disease. *Neurobiol Aging*. 2000;21(1):19–26. [https://doi.org/10.1016/S0197-4580\(99\)00107-4](https://doi.org/10.1016/S0197-4580(99)00107-4).
45. Padurariu M, Ciobica A, Mavroudis I, Fotiou D, Baloyannis S. Hippocampal neuronal loss in the CA1 and CA3 areas of Alzheimer's disease patients. *Psychiatr Danub*. 2012;24(2):152–8.
46. Wirths O, Bayer TA. Neuron loss in transgenic mouse models of Alzheimer's disease. *Int J Alzheimers Dis*. 2010;2010:1–6. <https://doi.org/10.4061/2010/723782>.
47. D'Amelio M, Cavallucci V, Cecconi F. Neuronal caspase-3 signaling: not only cell death. *Cell Death Differ*. 2010;17(7):1104–14. <https://doi.org/10.1038/cdd.2009.180>.
48. D'Amelio M, Sheng M, Cecconi F. Caspase-3 in the central nervous system: beyond apoptosis. *Trends Neurosci*. 2012;35(11):700–9. <https://doi.org/10.1016/j.tins.2012.06.004>.
49. Wang X, Wang W, Li L, Perry G, Lee HG, Zhu X. Oxidative stress and mitochondrial dysfunction in Alzheimer's disease. *Biochim Biophys Acta*. 2014;1842(8):1240–7. <https://doi.org/10.1016/j.bbdis.2013.10.015>.
50. Jena NR. DNA damage by reactive species: mechanisms, mutation and repair. *J Biosci*. 2012;37(3):503–17. <https://doi.org/10.1007/s12038-012-9218-2>.
51. Kruman II, Wersto RP, Cardozo-Pelaez F, Smilenov L, Chan SL, Chrest FJ, et al. Cell cycle activation linked to neuronal cell death initiated by DNA damage. *Neuron*. 2004;41(4):549–61. [https://doi.org/10.1016/S0896-6273\(04\)00017-0](https://doi.org/10.1016/S0896-6273(04)00017-0).
52. Herrup K, Busser JC. The induction of multiple cell cycle events precedes target-related neuronal death. *Development*. 1995;121(8):2385–95. <https://doi.org/10.1242/dev.121.8.2385>.
53. Counts SE, Mufson EJ. Regulator of cell cycle (RGCC) expression during the progression of Alzheimer's disease. *Cell Transplant*. 2017;26(4):693–702. <https://doi.org/10.3727/096368916X694184>.
54. van Leeuwen LA, Hoozemans JJ. Physiological and pathophysiological functions of cell cycle proteins in post-mitotic neurons: implications for Alzheimer's disease. *Acta Neuropathol*. 2015;129(4):511–25. <https://doi.org/10.1007/s00401-015-1382-7>.
55. Busser J, Geldmacher DS, Herrup K. Ectopic cell cycle proteins predict the sites of neuronal cell death in Alzheimer's disease brain. *J Neurosci*. 1998;18(8):2801–7. <https://doi.org/10.1523/JNEUROSCI.18-08-02801.1998>.
56. Dias-Santagata D, Fulga TA, Duttaroy A, Feany MB. Oxidative stress mediates tau-induced neurodegeneration in *Drosophila*. *J Clin Invest*. 2007;117(1):236–45. <https://doi.org/10.1172/JCI28769>.
57. Li L, Cheung T, Chen J, Herrup K. A comparative study of five mouse models of Alzheimer's disease: cell cycle events reveal new insights into neurons at risk for death. *Int J Alzheimers Dis*. 2011;2011:171464.
58. Meyer KD, Saletore Y, Zumbo P, Elemento O, Mason CE, Jaffrey SR. Comprehensive analysis of mRNA methylation reveals enrichment in 3' UTRs and near stop codons. *Cell*. 2012;149(7):1635–46. <https://doi.org/10.1016/j.cell.2012.05.003>.
59. Chan YW, Chen Y, Poon RY. Generation of an indestructible cyclin B1 by caspase-6-dependent cleavage during mitotic catastrophe. *Oncogene*. 2009;28(2):170–83. <https://doi.org/10.1038/onc.2008.369>.
60. Chen B, Ye F, Yu L, Jia G, Huang X, Zhang X, et al. Development of cell-active N6-methyladenosine RNA demethylase FTO inhibitor. *J Am Chem Soc*. 2012;134(43):17963–71. <https://doi.org/10.1021/ja3064149>.
61. Yu J, Chen M, Huang H, Zhu J, Song H, Zhu J, et al. Dynamic m6A modification regulates local translation of mRNA in axons. *Nucleic Acids Res*. 2018;46(3):1412–23. <https://doi.org/10.1093/nar/gkx1182>.
62. Murphy MP, LeVine H 3rd. Alzheimer's disease and the amyloid-beta peptide. *J Alzheimers Dis*. 2010;19(1):311–23. <https://doi.org/10.3233/JAD-2010-1221>.
63. Crews L, Masliah E. Molecular mechanisms of neurodegeneration in Alzheimer's disease. *Hum Mol Genet*. 2010;19(1):R12–20. <https://doi.org/10.1093/hmg/ddq160>.
64. Xiang Y, Laurent B, Hsu CH, Nachtergaele S, Lu Z, Sheng W, et al. RNA m(6) a methylation regulates the ultraviolet-induced DNA damage response. *Nature*. 2017;543(7646):573–6. <https://doi.org/10.1038/nature21671>.
65. Huang H, Camats-Perna J, Medeiros R, Anggono V, Widagdo J. Altered Expression of the m6A Methyltransferase METTL3 in Alzheimer's Disease. *eNeuro*. 2020;7(5).
66. Wen J, Lv R, Ma H, Shen H, He C, Wang J, et al. Zc3h13 regulates nuclear RNA m(6) a methylation and mouse embryonic stem cell self-renewal. *Mol Cell*. 2018;69(6):1028–38 e1026. <https://doi.org/10.1016/j.molcel.2018.02.015>.
67. Han M, Liu Z, Xu Y, Liu X, Wang D, Li F, et al. Abnormality of m6A mRNA methylation is involved in Alzheimer's disease. *Front Neurosci*. 2020;14:98. <https://doi.org/10.3389/fnins.2020.00098>.

68. Shafik AM, Zhang F, Guo Z, Dai Q, Pajdzik K, Li Y, et al. N6-methyladenosine dynamics in neurodevelopment and aging, and its potential role in Alzheimer's disease. *Genome Biol.* 2021;22(1):17. <https://doi.org/10.1186/s13059-020-02249-z>.
69. Tokarz P, Kaarniranta K, Blasiak J. Role of the cell cycle re-initiation in DNA damage response of post-mitotic cells and its implication in the pathogenesis of neurodegenerative diseases. *Rejuvenation Res.* 2016;19(2):131–9. <https://doi.org/10.1089/rej.2015.1717>.
70. Panneerdoss S, Eedunuri VK, Yadav P, Timilsina S, Rajamanickam S, Viswanadhapalli S, et al. Cross-talk among writers, readers, and erasers of m(6) A regulates cancer growth and progression. *Sci Adv.* 2018;4(10):eaar8263.
71. Klein JA, Ackerman SL. Oxidative stress, cell cycle, and neurodegeneration. *J Clin Invest.* 2003;111(6):785–93. <https://doi.org/10.1172/JCI200318182>.
72. Akiyama H, Barger S, Barnum S, Bradt B, Bauer J, Cole GM, et al. Inflammation and Alzheimer's disease. *Neurobiol Aging.* 2000;21(3):383–421. [https://doi.org/10.1016/S0197-4580\(00\)00124-X](https://doi.org/10.1016/S0197-4580(00)00124-X).
73. Mauer J, Jaffrey SR. FTO, m(6) Am, and the hypothesis of reversible epitranscriptomic mRNA modifications. *FEBS Lett.* 2018;592(12):2012–22. <https://doi.org/10.1002/1873-3468.13092>.
74. Akichika S, Hirano S, Shichino Y, Suzuki T, Nishimasu H, Ishitani R, et al. Cap-specific terminal N (6)-methylation of RNA by an RNA polymerase II-associated methyltransferase. *Science.* 2019;363(6423).

Publisher's Note

Springer Nature remains neutral with regard to jurisdictional claims in published maps and institutional affiliations.

Ready to submit your research? Choose BMC and benefit from:

- fast, convenient online submission
- thorough peer review by experienced researchers in your field
- rapid publication on acceptance
- support for research data, including large and complex data types
- gold Open Access which fosters wider collaboration and increased citations
- maximum visibility for your research: over 100M website views per year

At BMC, research is always in progress.

Learn more biomedcentral.com/submissions

